A biomimic anti-neuroinflammatory nanoplatform for active neutrophil extracellular traps targeting and spinal cord injury therapy

Chunming Tang [b,1], Yaoyao Jin [d,1], Min Wu [b,1], Feng Jia [e,1], Xiaowei Lu [f], Jinyu Li [b], Jie Wu [b], Senlin Zhu [b], Zhiji Wang [b], Di An [a], Wu Xiong [c], Yongjie Zhang [c,**], Huae Xu [b,*], Xufeng Chen [a,***]

[a] Department of Emergency Medicine, The First Affiliated Hospital of Nanjing Medical University, Nanjing, 210029, China
[b] Department of Pharmaceutics, School of Pharmacy, Nanjing Medical University, Nanjing, 211166, China
[c] Department of Human Anatomy, Nanjing Medical University, Nanjing, 211166, China
[d] Department of Emergency, The Affiliated Huai'an Hospital of Xuzhou Medical University and The Second People's Hospital of Huai'an, Huai'an, 223022, China
[e] Department of Neurosurgery, Yancheng NO.1 People's Hospital, The Affiliated Yancheng First Hospital of Nanjing University Medical School, Yancheng, 224008, China
[f] Department of Geriatric Neurology, the First Affiliated Hospital of Nanjing Medical University, Nanjing, 210029, China

ARTICLE INFO

ABSTRACT

Traumatic spinal cord injury (SCI) always leads to severe neurological deficits and permanent damage. Neuro-inflammation is a vital process of SCI and have become a promising target for SCI treatment. However, the neuroinflammation-targeted therapy would hinder the functional recovery of spinal cord and lead to the treatment failure. Herein, a biomimic anti-neuroinflammatory nanoplatform (DHCNPs) was developed for active neutrophil extracellular traps (NETs) targeting and SCI treatment. The curcumin-loaded liposome with the anti-inflammatory property acted as the core of the DHCNPs. Platelet membrane and neutrophil membrane were fused to form the biomimic hybrid membrane of the DHCNPs for hijacking neutrophils and neutralizing the elevated neutrophil-related proinflammatory cytokines, respectively. DNAse I modification on the hybrid membrane could achieve NETs degradation, blood spinal cord barrier, and neuron repair. Further studies proved that the DHCNPs could reprogram the multifaceted neuroinflammation and reverse the SCI process via nuclear factor kappa-B (NF-κB) pathway. We believe that the current study provides a new perspective for neuro-inflammation inhibition and may shed new light on the treatment of SCI.

1. Introduction

Traumatic spinal cord injury (SCI) is a catastrophic neuronal injury leading to severe neurological deficits and permanent damage with high disability and mortality rate [1]. Traumatic SCI pathophysiology involves a primary injury and a subsequent secondary injury. The primary injury occurs when an external mechanical force compresses or transects the spinal cord, followed by the secondary injury by a series of complex cellular cascades with damage propagation [1,2]. The existing clinical therapeutic approaches, including hemodynamic support, decompressive surgery (within 24 h), and therapeutic hypothermia, all remain controversial and fail to mitigate the progressive secondary injury [3,4].

Among these detrimental secondary cascades, neuroinflammation has come into the focus of research because of its key role in regulating the pathogenesis of SCI. Since primary injury happens unexpectedly, targeting neuroinflammatory is crucial for alleviating neurological dysfunction after SCI happening [5,6].

Neuroinflammatory responses are mainly characterized by the influx of multiple immune cells (e.g., neutrophils (NEs), monocytes, and lymphocytes) via the broken blood-spinal cord barrier (BSCB) [7,8]. The infiltrating immune cells reach the injured site rapidly and are capable of secreting excessive proinflammatory cytokines, chemokines, reactive oxygen species (ROS), and nitric oxide to exacerbate inflammation and worsen the SCI [9]. Currently, early administration of

methylprednisolone, a kind of glucocorticoid steroid, is the only clinically recommended anti-neuroinflammatory therapeutic modality. However, methylprednisolone has several serious side effects, including gastrointestinal hemorrhage, thromboembolism, sepsis, infections, and immune depression, which largely weaken the therapeutic outcomes of SCI [10,11]. Importantly, although the recruited immune cells by neuroinflammatory are associated with tissue damage, they also play an important role in the debris clearance and tissue function recovery, resulting in the complicated roles of neuroinflammatory [12,13]. Thus, developing combinatorial treatment strategies to precisely regulate the complex, multifaceted neuroinflammatory processes could facilitate the therapy of traumatic SCI.

Among the numerous kinds of immune cells involved in the neuroinflammatory processes, mounting evidence suggests that neutrophil plays a pivotal role in the pathophysiology of SCI [14]. When neuroinflammatory occurs, neutrophils are typically the first cells to infiltrate the injured spinal cord. While the role of neutrophils in SCI pathophysiology remains debated, these infiltrating neutrophils are associated with excessive production of ROS, pro-inflammatory mediators, and cytokines (e.g., TNF-α, IL-1β, and IL-6), which exacerbate neurological deficits [15,16]. In addition to secreting cytotoxic products, activated neutrophils can also form neutrophil extracellular traps (NETs) by releasing granular proteins and chromatin within a DNA framework. While NETs are commonly regarded as a response mechanism against extracellular pathogens to enhance antimicrobial activity, accumulating evidence shows NETs formation in various inflammatory central nervous system (CNS) diseases, including ischemic stroke, intracerebral hemorrhage, multiple sclerosis and traumatic brain injury (TBI), and this phenomenon may contribute to the blood-brain barrier damage and neural injury [17–21]. A recent study has revealed that excess NETs have been implicated in promoting neuroinflammation and disrupting the BSCB, thereby exacerbating secondary injury during SCI [22]. Consequently, targeting NETs presents a promising avenue for alleviating NETs-mediated neurological damage and facilitating functional recovery in the treatment of SCI.

The formation and degradation of NETs is a dynamic process, with DNase I being one of the key enzymes involved. DNase I, a nuclease that degrades both single- and double-stranded DNA, is abundant in biological systems. It hydrolyzes phosphodiester bonds in DNA strands, breaking down DNA into smaller oligonucleotides and mononucleotide fragments [23,24]. This degradation helps regulate the balance of NETs in the body, preventing tissue damage and inflammatory responses caused by their excessive accumulation. Multiple studies have shown that using DNase I to degrade NETs can significantly reduce inflammation and tissue damage after acute spinal injury, promoting neurological recovery. However, its application is limited by drawbacks such as poor stability, short half-life, low bioavailability, and limited penetration and accumulation capabilities. To overcome these limitations, nanotechnology has emerged as a promising approach to enhance the stability, bioavailability, and targeted delivery of DNase I, thereby improving its therapeutic potential for managing NETs [25–27].

Recently, biomimetic nanoplatforms derived from various kinds of cell membranes have gained increasing attention for the delivery of therapeutic agents, providing them with a wide range of biofunctions such as improved biocompatibility and disease-relevant targetability [28]. Our previous studies indicated that the platelet membrane-camouflaged nanomedicine could selectively identify and target inflammatory neutrophils for the diagnosis and treatment of neuroinflammation induced by ischemic stroke [29]. Additionally, neutrophil membrane-coated nanoparticles show promise in treating rheumatoid arthritis by neutralizing proinflammatory cytokines and suppressing synovial inflammation [30].

Herein, inspired by the intrinsic targeting abilities of platelet and neutrophil membranes, Deoxyribonuclease I (DNAse I)-modified hybrid membrane-coated nanoparticles (DHCNPs) were developed to modulate the neuroinflammatory microenvironment by eliminating NETs and decreasing proinflammatory cytokines for effective SCI treatment (Scheme 1). The curcumin (Cur)-loaded liposomes (CLs) acted as core of the DHCNPs for the inhibition of the neuroinflammatory-induced inflammation [31]. The platelet-neutrophil hybrid membrane vesicles (DHVs) were coated on the CLs for hijacking neutrophils and neutralizing the proinflammatory cytokines. Besides, the DHVs were decorated with DNAse I for the degradation of NETs. *In vitro* and *in vivo* studies demonstrated the prepared biomimic anti-inflammatory DHCNPs could degrade the neuroinflammation-induced NETs, protect the BCSB, reprogram the multifaceted neuroinflammatory processes, and finally achieve highly efficient SCI treatment in the spinal cord contusion mouse models.

2. Materials and methods

2.1. Preparation and characterization of DNAse I conjugated neutrophils

Mature neutrophils were isolated from murine bone marrow as described previously [32]. In brief, the femur and the tibia from both hind legs were immersed in RPMI 1640 medium after removal of the muscle and sinew. The bone marrow was flushed from the bone with HBSS-EDTA solution, centrifuged at 200 g for 3 min and resuspended in 1 mL of HBSS-EDTA. The cells were laid on a Percoll mixture solution consisting of 55 %, 65 % and 75 % Percoll, followed by centrifugation at 1500g for 30 min. The mature neutrophils were recovered at the interface of the 65 % and 75 % fractions and washed with ice-cold HBSS-EDTA thrice.

The surface of the neutrophils was functionalized with DNAse I in three steps [33]. First, obtained neutrophils (2×10^6) was resuspended in 1 mL of PBS, and incubated with 1 mM of TCEP (Sigma) for 20 min at 37 °C. After incubation, the excess TCEP was removed by centrifugation at 1000g for 4 min and washed with PBS thrice. For the certification of active thiols on surface of neutrophils, Ellman's assay (Aladdin) was performed following the manufacturer's procedure. Fluorescent dye with a maleimide functional group (Cy5 maleimide) was utilized to evaluate the coating efficiency. After TCEP treatment, neutrophils were washed with PBS thrice, and incubated with 10 μg/mL of Cy5 maleimide for 20 min at 37 °C. After incubation, Hoechst 33342 was used to stain the nuclei for 15 min. Subsequently, the cells were washed with PBS and fixed with 4 % paraformaldehyde for 15 min before imaging under a confocal laser scanning microscope (CLSM, LSM 880, Zeiss).

In the meantime, DNAse I was mixed with sulfosuccinimidyl-4-(N-maleimidomethyl)-cyclohexane-1-carboxylate (Sulfo-SMCC) (Sigma) in PBS at a molar ratio of 1:1.2 for 2 h at 4 °C. The excess Sulfo-SMCC was removed using a centrifugal filter device (molecular weight cut-off = 10 kDa) to purify the SMCC activated DNAse I. Lastly, TCEP treated neutrophils were incubated with SMCC activated DNAse I for 1 h at room temperature, the unconjugated DNAse I was removed by centrifugation at 1000g for 4 min. The resulting DNAse I conjugated neutrophils were treated with 10 μM fMLF (Sigma) for 10 min at 37 °C, washed with PBS thrice and were stored at 37 °C prior to use in experiments. To image the DNAse I on neutrophil membranes, fluorescently labeled neutrophils were prepared with the similar method described above except using Alexa Fluor™ 488-DNAse I (Invitrogen) instead of DNAse I.

2.2. Preparation and characterization of DHVs

DNAse I conjugated neutrophil vesicles (DNVs) and platelet vesicles (PVs) were prepared according to our previously described protocols [29,32]. For membrane fusion, DNVs and PVs were mixed at a protein weight ratio of 1:1, followed by stirring at 37 °C for 10 min to facilitate the fusion of the two vesicles. After that, the mixture was treated with sonication and mechanical extrusion to obtain the resulting DHVs.

To explore membrane fusion process, two FRET dyes were employed via the established protocol [34]. Briefly, neutrophil membrane was stained with DiD and DiI, and platelet membrane was then added to the
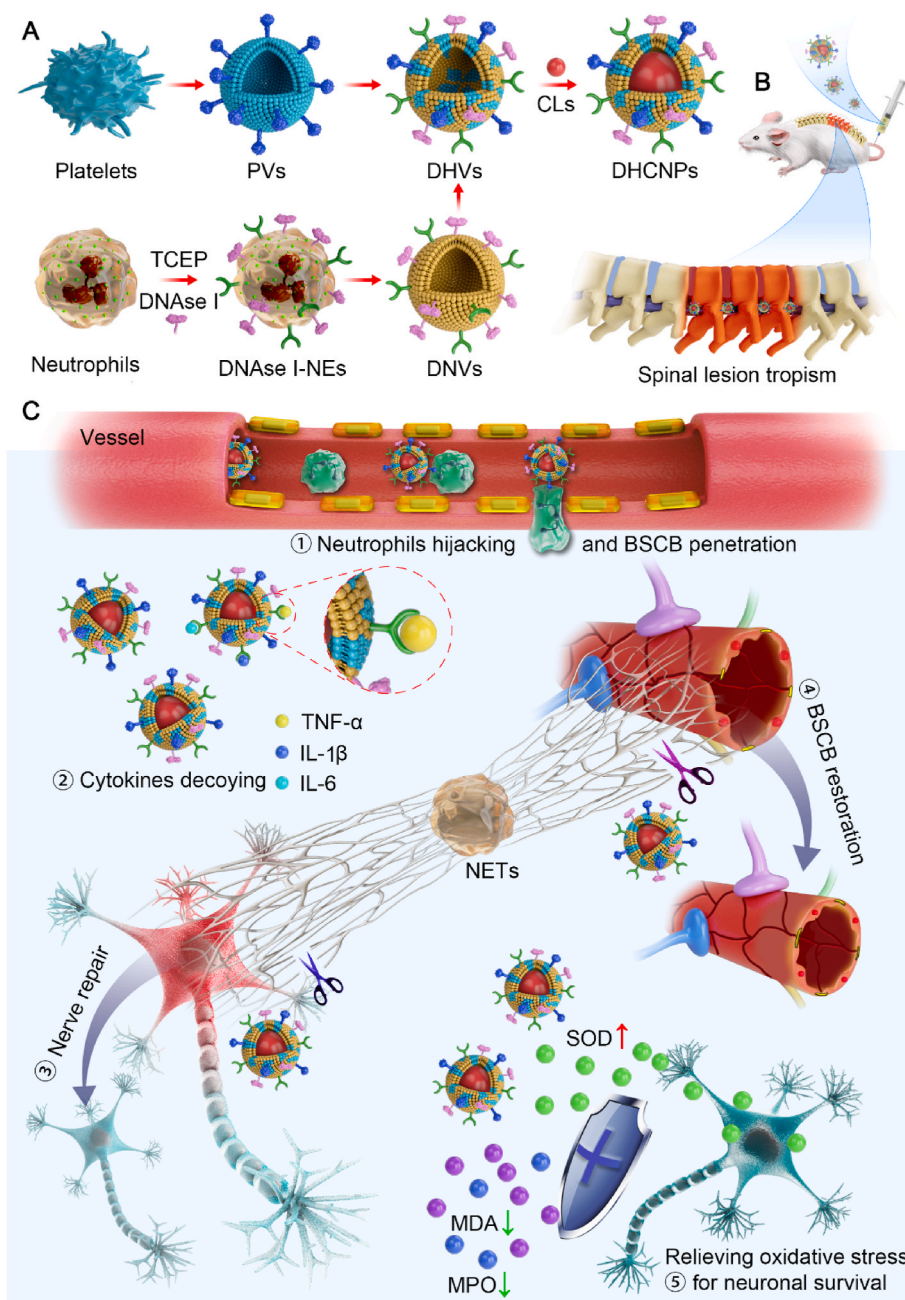
Scheme 1. (A) Scheme of the fabrication of DHCNPs. (B) DHCNPs exhibited neuroinflammation tropism to injured spinal cord after intravenous injection. (C) The neuroinflammatory and SCI modulation process of the DHCNPs.

DiD/DiI-doped neutrophil membrane at weight ratios of 0:1, 1:1, 3:1, and 5:1. The fluorescence spectrum was then recorded between 550 and 750 nm with excitation wavelength at 525 nm by a Tecan Infinite M200 plate reader. The fluorescence recovery of the donor (DiI) was used to indicate increasing amounts of fusion. To conduct the membrane colocalization study, DiI-dyed neutrophil membranes and DiO-dyed platelet membranes were fused or physically mixed, followed by being visualized under CLSM (LSM 880, Zeiss).

2.3. Preparation and characterization of DHCNPs

Membrane-coated nanoparticles were fabricated by a previously reported sonication method [30]. Briefly, curcumin-loaded liposome cores were prepared using a modified thin-film hydration method. The curcumin, SPC, cholesterol, DSPE-PEG (1:25:4:4, w:w) were dissolved in the mixture of chloroform and methanol (2:1, v:v) and evaporated to form a thin film in a round flask. After vacuum dry overnight, the lipid film containing Cur was hydrated with the distilled water at 37 °C. The resulting liposome solution was sonicated using a probe type sonicator at 150 w for 10 min in ice bath and sequentially extruded through the membrane filters with a pore size of 0.45 and 0.22 μm. The Cy5 labeled liposomes were prepared with the similar method described above except using 0.1 wt% Cy5 instead of curcumin. Afterward, A mixture of liposome cores and fused hybrid membranes at a membrane protein/liposome weight ratio of 1:2 was sonicated using a bath sonicator for 3 min to synthesize the resulting DHCNPs.

The particle size and surface zeta potential of CLs, PVs, DNVs and DHCNPs were characterized using dynamic light scattering (DLS), respectively. The morphologies were determined by a transmission electron microscopy (TEM, JEM-200CX, JEOL, Japan). The samples

were prepared by contacting the nanoparticle droplets at a concentration of 100 μg/mL with copper grids for 3 min, and staining by 1 % uranyl acetate for 30 s before the TEM visualization. To evaluate the stability, CLs and DHCNPs were suspended in either in 1 × PBS for 14 d or 100 % FBS for 24 h at a final concentration of 1 mg/mL. During the course of test, the changes of size were measured by DLS. To study the Cur release efficiency, the mixture of 0.5 mL CLs or DHCNPs and 0.5 mL 2 × FBS were added into a dialysis tube (3.5K MWCO) embedded into 50 mL of the PBS buffer solution (pH = 7.4) containing Tween 80 (1 %, w:v), and gently shaken at 37 °C in a shaker at 100 rpm. At predetermined time intervals, 1 mL of the medium was drawn out and replaced with an equal volume of fresh medium. Then, Cur was extracted and measured to determine the release profile of Cur using high performance liquid chromatography (HPLC, LC-2010AHT, SHIMADZU, Japan).

To determine the enzyme activity of DNAse I, 10 μg/mL DNA plasmid sample was filled in the 96-well plate and incubated with DHCNPs (1 μg DNAse I) at 37 °C for 30 min. As a control, free DNAse I (1 μg), HCNPs (without conjugated DNAse I) and physically mixture of HCNPs and DNAse I (1 μg) were also tested. Following the incubation, absorbance was measured at 260 nm using multimode plate reader (Synergy HTX, Biotek). Finally, the % hydrolytic activity of DNAse-I and DHCNPs was calculated. Coomassie blue staining was employed to identify the membrane proteins retained on DNVs, PVs and DHCNPs. Briefly, the samples containing equivalent total proteins measured by BCA protein assay kit (Life Technologies) were added to the 10 % SDS-polyacrylamide gel to separate different molecular weights of proteins. Subsequently, the resulting polyacrylamide gel was stained with Commassie blue and imaged. The key membrane proteins were identified by western blotting using primary antibodies specific to the target protein. To quantify inflammatory factors binding capability, recombinant mouse TNF-α (8 ng/mL, Thermo Fisher Scientific) or IL-1β (10 ng/mL, Thermo Fisher Scientific) were incubated with DHCNPs (0−4 mg/mL) for 2 h at 37 °C. The mixtures were then centrifuged at 20000 g for 20 min to remove the nanoparticles. The cytokine concentration in the supernatant was quantified by mouse TNF-α or mouse IL-1β enzyme-linked immunosorbent assay (ELISA) kits (elabscience). Nonlinear fitting of curves was performed in GraphPad Prism 7 software.

2.4. In vitro cytotoxicity assay

Pre-stimulated neutrophils (1×10^4 cells/well) were seeded in 96-well plates and cultured in the FBS free medium for 30 min. Afterward, cells were treated with different concentrations (i.e., 10, 25, 50, 100, 200, 500 and 1000 μg/mL) of CLs and DHCNPs for 2 h, taking the blank medium as blank controls. Cell viabilities were measured by CCK-8 assay with the absorbance determined through a microplate reader at the wavelength of 450 nm.

2.5. Animals

C57BL/6 mice (female, 8–10 weeks) were maintained in a constant environment (ambient temperature 22 ± 2 °C, humidity 45 ± 5 %, and a 12 h light/dark cycle) in the Animal Research Center at Nanjing Medical University. All animal experiments were approved by the Institutional Animal Care and Use committee of the Nanjing Medical University (IACUC:1809007).

2.6. Mice model of SCI

A contusive SCI on mice was produced at the 9th thoracic vertebral level using the Louisville Injury System Apparatus (LISA) impactor as described [35]. Briefly, mice were anesthetized with pentobarbital (40 mg/kg; intraperitoneally) and placed on a sterile operating table to expose spinal cord by T9 laminectomy surgery. Then, the exposed spinal cord was injured using a LISA impactor with a displacement of 0.6 mm.

Subsequently, the muscles and skin were sutured in layers with surgical suture and the mice were placed in a temperature- and humidity-controlled cage until they recovered from anesthesia. After surgery, mice received intraperitoneal injection of gentamicin daily for 1 week, and manual bladder expression twice daily until reflex bladder emptying was established. All the groups were performed and quantified in a randomized fashion by investigators blinded to treatment groups.

2.7. Recognition of DHCNPs by neutrophils in blood

SCI mice were intravenously injected with FITC-labeled DHCNPs or FITC-labeled CLs at a FITC dose of 30 nmol/kg at 1 h post injury. 2 h after injection, whole blood samples were collected for the isolation of neutrophils using the density gradient centrifugation method based on a previous study [32]. The obtained cells were fixed and visualized under CLSM (LSM 880, Zeiss) and further analyzed by flow cytometry (AccuriC6, BD, USA). The mice injected with saline were used as control group.

2.8. In vivo fluorescence images

To study the distribution and targeting properties of DHCNPs, SCI mice were randomly divided into four groups and intravenously injected with saline, free DiR, DiR-labeled CLs and DiR-labeled DHCNPs at a DiR dose of 20 nmol/kg. Images of the mice were taken on *in vivo* imaging system (PerkinElmer, USA) at 2, 4, 8 and 12 h post injection. The spinal cord area fluorescence intensity of each mouse was analyzed by Living Image Software. In addition, the spinal cords, hearts, livers, spleens, lungs, and kidneys were acquired at each time point and subjected for *ex vivo* imaging. The fluorescence intensities of region-of-interests (ROI) were analyzed by Living Image Software.

2.9. In vivo two-photon imaging

In vivo intravital microscopy of mouse spinal cord was performed as reported [36]. Briefly, the surface of the injured spinal cord was covered with a sterile cover glass and fixed with dental cement. RhB-labeled CLs and RhB-labeled DHCNPs were administered immediately, and 4 h later, mice were imaged through spinal cord windows using a two-photon laser-scanning microscope (Zeiss LSM 780, Germany) with an a × 20/1.0 NA water immersion objective lens and a high-speed camera. 15 mins before observation, 100 μL of 10 mg/mL FITC-dextran (2,000K Da, Sigma-Aldrich) was injected intravenously to label vessels of the spinal cords. The mice injected with saline were used as control group. During imaging, all mice were placed on a thermo-controlled blanket at 37 °C on an intravital microscope tray and under anesthesia with 1.5 % iso-flurane in 30 % oxygen and 70 % nitrous oxide.

To visualize NETs, mice were intravenously injected with 5 μL Sytox green (Invitrogen) 30 min before imaging. Z-stacks were taken and Sytox green-positive single NET fibers were counted using Image J. Data are presented as the average number of fibers per mm^2 of spinal cord tissue. Sytox green positive intact cells were excluded from the quantification [37].

2.10. In vivo targetability and therapeutic efficacy assay

To study *in vivo* targetability of DHCNPs to neutrophils in injured spinal cord, FITC-labeled CLs and FITC-labeled DHCNPs were intravenously administered to SCI mice at 1 h post injury. The mice injected with saline were used as control group. Approximately 4 h later, mice were sacrificed and the spinal cord tissues were harvested for subsequent immunofluorescent staining. To evaluate the therapeutic efficacy of nanoparticles with SCI mice, 200 μL of saline, HCNPs, DHNPs and DHCNPs (~5 mg curcumin/kg, 1 mg DNAse I/kg) were intravenously injected on hours 1, 12 and 24 after spinal cord injury. An untreated sham group was used as the negative control. The Basso mouse scale

(BMS) score was recorded at 1, 3, 5, 7, 14, 21 and 28 days postinjury. Mice were sacrificed and the blood, spinal cord tissues, and major organs were harvested at day 28th later for subsequent examinations. Luxol fast blue (LFB) and immunofluorescent staining was employed to identify demyelination and glial scar formation. H&E histological and hematological analysis were used to evaluate the biomedical safety. For further evaluation, the same dose of nanoparticles was injected at 1 and 12 h after SCI. Mice were sacrificed at 24 h postinjury and plasma and spinal cords of the injured site were collected for subsequent evaluation experiments.

Immunofluorescent staining was employed to determine neutrophil NETs degradation and nerve repair. Enzyme-linked immunosorbent assay (ELISA) was employed to evaluate the anti-inflammatory and antioxidant activity of DHCNPs. Briefly, spinal cords of the injured site were collected and the levels of inflammatory cytokines (TNF-α, IL-1β, IFN-γ, IL-6, IL-10, and IL-4) and oxidative stress-related factors superoxide dismutase (SOD), malondialdehyde (MDA), and myeloperoxidase (MPO) in the collected tissues were determined by ELISA following the manufacturer's instructions. Western blot was used to analyze the H3Cit, cleaved caspase-3, zona occludens-1 (ZO-1) and Occludin level. Briefly, total protein of the spinal cord tissues was extracted with RIPA lysis buffer (Millipore) containing protease inhibitor cocktails (Roche) according to the manufacturer's instructions. The samples containing equivalent total proteins were loaded on SDS-polyacrylamide gel electrophoresis gels and transferred onto polyvinylidene difluoride membranes. Primary antibodies against H3Cit (Abcam), p-IκBα (Thermo), IκBα (Thermo), cleaved caspase-3 (Abcam), ZO-1 (Abcam) or Occludin (Abcam) were used. Immunoreactive bands were visualized with Tanon 5200 Multi Chemiluminescence Imaging System and analyzed with Image J. DNA quantification kit was used to determine plasma DNA. Briefly, Plasma was collected from whole blood by centrifugation at 150g for 15 min. DNA in plasma was quantified according to the manufacturer's instructions using the Quant-iT PicoGreen dsDNA Assay kit (Invitrogen). Evans blue (EB) was used to monitor blood spinal cord barrier (BSCB) permeability as previously described with modifications [22]. Briefly, 24 h after SCI, mice were intravenously injected with 4 % EB dye (4 mL/kg; Sigma-Aldrich). One hour later, mice were perfused with PBS, and injured spinal cord were weighted and homogenized. After centrifugation, optical density of supernatants was measured by spectrophotometry at 620/680 nm. For EB fluorescence, injured spinal cord was fixed with 4 % paraformaldehyde, sectioned into 10 mm slices and visualized under CLSM (LSM 880, Zeiss).

2.11. Immunofluorescent staining

The spinal cords were removed with perfusion and fixed in 4 % formaldehyde, followed by dehydrating in 20 % sucrose and then in 30 % sucrose. After dehydration, the spinal cords were frozen with O.C.T at −80 °C and sections (14 μm) were cut on a freezing microtome (Leica CM1520, Germany). Primary antibodies against Ly6G (BD Pharmingen), glial fibrillary acidic protein (GFAP) (Millipore), H3Cit (Abcam), NeuN (Abcam) were used. The nucleus was stained with DAPI. Staining sections were visualized using a confocal microscope (LSM 880, Zeiss, Germany). The numbers of Ly6G-positive and H3Cit-positive cells in the traced area were determined.

2.12. Behavioral assessments

The Basso mouse scale (BMS) scoring system was used to assess the recovery of locomotor functions of SCI mice at 1, 3, 5, 7, 14, 21 and 28 days postinjury [38]. Briefly, each mouse was placed in an open field and observed for 5 min by two observers who were blinded to the experimental groups. The movements were scored based on the joint movement, weight support, plantar stepping, paw position, coordination, and trunk and tail control following the standard guide. Motor function was evaluated according to the 0–9 BMS scoring.

2.13. In vitro NETs degradation evaluation

NETs were induced by the stimulation of neutrophils with phorbol 12-myristate 13-acetate (PMA) as previously reported [39]. Briefly, 1×10^6 isolated neutrophils were plated in 6-well culture plates and incubated at 37 °C for 30 min. Then, PMA was added (1 μM final concentration) into the medium to induce the formation of NETs. The medium containing PMA was discarded, and NETs were washed with PBS carefully. Afterward, DNAse I or DHCNPs (at a DNAse I dose of 500 μg/mL) were added and cultured. After 2 h of incubation, SYTOX green nucleic acid stain (500 nM, Thermo Fisher Scientific) was added into the well. After washing, the samples were fixed with Vectashield containing DAPI and visualized under CLSM (LSM 880, Zeiss). Moreover, for fluorescence intensity quantification, SYTOX green single-channel images were analyzed using Image J.

2.14. Bioluminescence image of NF-κB activation

The NF-κB-luc reporter mice were sourced from Caliper Life Sciences (Hopkinton, USA). Prior to fabricating contusive SCI models, the mice were anesthetized using 1.25 % tribromoethanol. Subsequently, the mice were randomly assigned to receive intravenous injections of either saline, HCNPs, DHNPs, or DHCNPs. 2 days later, bioluminescence images were captured. Following intraperitoneal administration of D-luciferin for 30 min, the in vivo imaging system was employed to detect luciferase signals. The fluorescence intensities of the ROI were then analyzed using the Living Image Software.

2.15. In vitro neuroprotetive effects of DHCNPs on NETs trapped neurons

Primary spinal cord neurons were isolated from pregnant mice as previously described [40]. Briefly, pregnant mouse was anesthetized and sacrificed, and all embryos were separated under aseptic conditions. Under dissection microscope, the spinal cord was isolated from each embryo and the membrane of the spinal cord and dorsal root ganglion was removed. Subsequently, the spinal cord was quickly cut into small pieces and digested with 0.25 % trypsin at 37 °C and 5 % CO$_2$ for 30 min. Cell suspension was obtained by filtration with a 100 μm cell strainer. The obtained primary spinal cord neurons were cultured in complete basal medium (Neural basal + B27 + 2 % glutamate) for 10 days. Afterwords, generated NETs were added and treated with DNAse I or DHCNPs (at a DNAse I dose of 100 μg/mL). After 12 h of incubation, neuronal viability was assessed with NeuN staining. The numbers of NeuN-positive cells were determined.

2.16. Statistical analysis

Data are presented as mean ± standard deviation. The statistically significant differences were assessed by two-tailed unpaired Student's t-test, one-way or two-way analysis of variance (ANOVA) with Tukey's multiple comparisons test. All statistical analyses were performed using GraphPad Prism software and data were considered to be statistically significant when $P < 0.05$. n. s., not significant, *$P < 0.05$, **$P < 0.01$, ***$P < 0.001$, ****$P < 0.0001$.

3. Results

3.1. Preparation and characterization of DHCNPs

The DHCNPs were composed of CLs as inner core and DNAse I-modified hybrid membrane as the coating shell. To prepare the DHCNPs, neutrophils were first engineered with DNAse I via a bifunctional maleimide linker [41]. Briefly, the neutrophils were pretreated with tris (2-carboxyethyl)phosphine (TCEP), to expose active thiols, and then were coupled with maleimide-DNAse I through thiol-maleimide reaction. The expression of active thiols on neutrophil surface was validated

using Ellman's assay and immunofluorescence staining (Fig. S1), respectively. Alexa Fluor™ 488-labled DNAse I was applied to confirm the conjugation process, and the green fluorescence of Alexa Fluor™ 488 on the neutrophil illustrating the successful conjugation of DNAse I on neutrophil membranes (Fig. S2). Next, the engineered neutrophils underwent hypotonic swelling and physical homogenization to obtain DNAse I conjugated neutrophil vesicles (DNVs). Then, platelets were

collected and subjected to repeated freeze-thaw cycles to obtain platelet vesicles (PVs), which were fused with DNVs to fabricate DHVs through a sonication and extrusion process [42]. To confirm the successful fabrication of the hybrid vesicle, DNVs were labeled with a Förster resonance energy transfer (FRET) pair of dyes and fused with different amounts of PVs. With the increase of PVs, the fluorescence intensity (FI) was increased at 576 nm and decreased at 670 nm (Fig. 1A), owing to
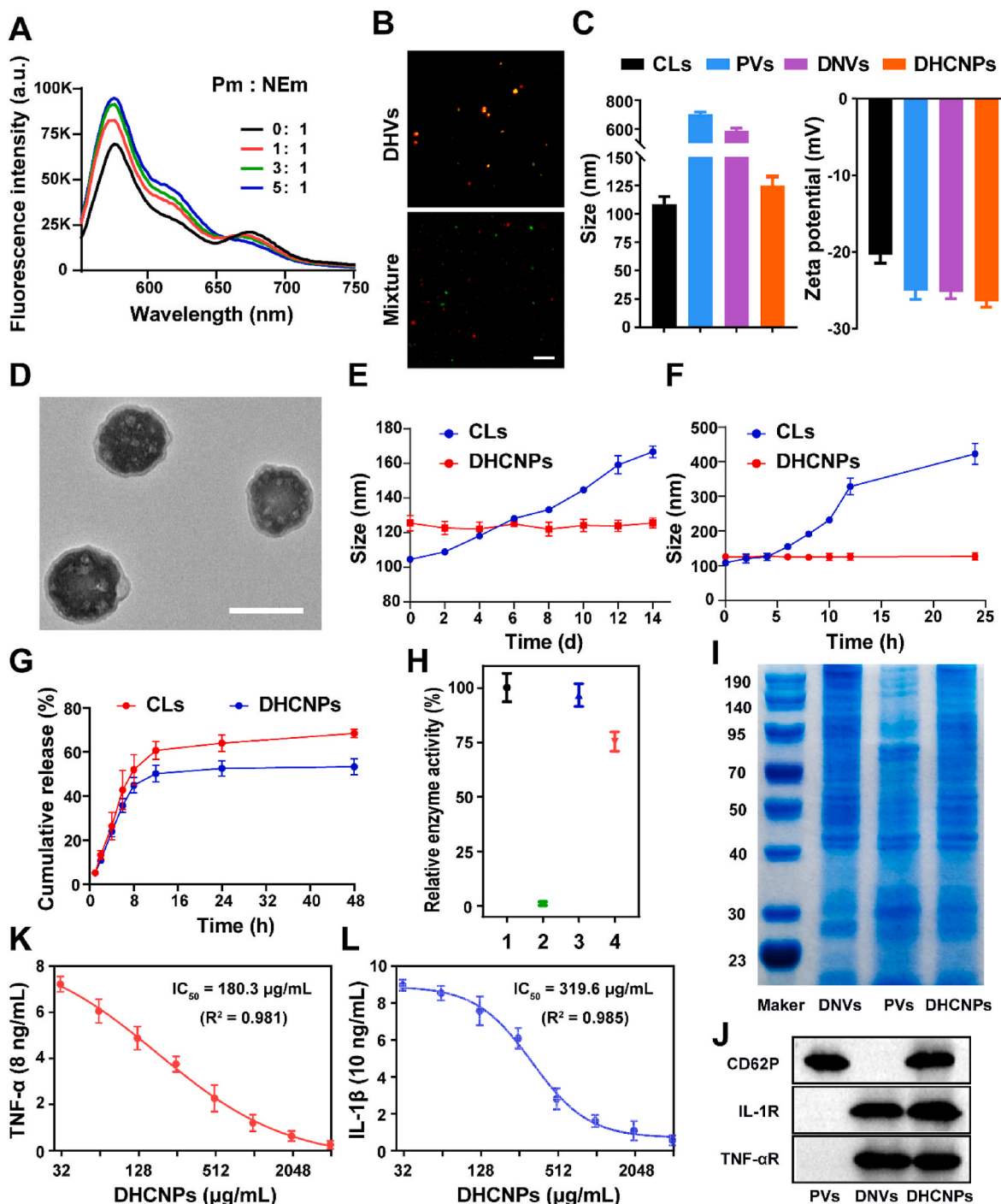

Fig. 1. Characterizations of the DHCNPs. (A) The recovery of fluorescence emission at the lower emission wavelength around 576 nm. *Pm*: NEm means the weight ratio of platelet membrane to neutrophil membrane. (B) Confocal fluorescence images of DHVs (top) and physical mixture of DNVs and PVs (bottom). Red: DNVs doped with Dil dye; green: PVs doped with DiO dye. Scale bar: 10 μm. (C) DLS results and zeta potentials of the CLs, PVs, DNVs, and DHCNPs, respectively. (D) TEM image of DHCNPs. Scale bar: 100 nm. Long-term stability of CLs and DHCNPs in PBS (E), and 100 % FBS (F) (n = 3). (G) *In vitro* release of Cur from CLs and DHCNPs in FBS (n = 3). (H) Enzyme activity assay of free DNAse I (1), HCNPs (2), HCNPs + free DNAse I (3), and DHCNPs (4) (n = 3). (I) SDS-PAGE analysis of retention proteins from DNVs, PVs, and DHCNPs. (J) Western blot assay of CD62P, IL-1R, and TNF-αR in PVs, DNVs, and DHCNPs. (K, L) Binding capacity of DHCNPs with TNF-α and IL-1β examined by ELISA (n = 3).

the interspersing of the two kinds of membranes weakened the FRET interaction in the original DNVs, indicating the successful fusion. The successful fusion of two different cell membranes was also verified through colocalization of DiI-labeled DNVs and DiO-labeled PVs. As shown in Fig. 1B, the fluorescence of DiI and DiO colocalized well in the hybrid membrane sample. In contrast, the physical mixture of the two kinds of membranes without any extrusion showed distinct green and red fluorescence spots. Then, CLs were prepared using a thin-film dispersion method, and DHCNPs were fabricated by fusing DHVs onto the surface of CLs through a sonication process.

The dynamic light scattering (DLS) indicated that the DHCNPs had an average particle size of 128.4 nm, which was 15 nm larger than the uncoated CLs. The Zeta potential of DHCNPs and the hybrid vesicle were measured to be −26.2 mV and −25.8 mV, respectively. The drug loading rate and encapsulation efficiency of Cur were 2.64 % and 83.7 %, respectively (Fig. 1C and Table S1). Furthermore, the transmission electron microscopy (TEM) images showed a core-shell structure of DHCNPs, displaying a unilamellar membrane over their liposomal cores (Fig. 1D and S3). To investigate the colloidal stability of DHCNPs, the size change of DHCNPs in phosphate buffered saline (PBS) and 100 % foetal bovine serum (FBS) was evaluated over time (Fig. 1E and F). Compared to CLs, DHCNPs exhibited improved colloidal stability, suggesting the protective effect of the hybrid membrane. In addition, the delayed release of Cur from DHCNPs in serum suggested that the hybrid membrane could act as a diffusion barrier to slow down the drug diffusion rate (Fig. 1G). To verify the enzyme activity of the conjugated DNAse I, DNA plasmid was incubated with DHCNPs and the hydrolytic activity was measured using a microplate reader (Fig. 1H). Compared with free DNAse I (100 % activity), DHCNPs displayed promising enzymatic hydrolysis of the DNA (around 75.4 %), indicating DNAse I grafted on DHCNPs retained its enzyme activity.

The aim of coating the hybrid membrane was to mimic the neutrophil hijacking and proinflammatory cytokines neutralizing properties of platelets and neutrophils, respectively, which were strongly related with the cell membrane proteins. Thus, the protein profiles of DHCNPs were analyzed by sodium dodecyl sulfate-polyacrylamide gel electrophoresis (SDS-PAGE) (Fig. 1I). It was found that the profile of proteins tracked on DHCNPs was the union of two single membrane formulations. Western blotting was further used to confirm the presence of critical receptor proteins of the two kinds of membranes such as CD62P, TNF-α receptor (TNF-αR), and IL-1 receptor (IL-1R) on DHCNPs (Fig. 1J), further reflecting the successful translocation of platelet and neutrophil membrane proteins onto DHCNPs. Studies have shown that the outer neutrophil membrane proteins (e.g., TNF-αR and IL-1R) could make the neutrophil membrane-coated nanoparticles act as decoys to neutralize proinflammatory cytokines and relieve overwhelming inflammation [30]. Next, we evaluated whether DHCNPs could adsorb proinflammatory cytokines, such as TNF-α and IL-1β *in vitro*, which play crucial roles in initiating neuroinflammation and promoting SCI progression [9]. To evaluate the affinity of DHCNPs for these cytokines, the binding kinetic profiles were measured using enzyme-linked immunosorbent assay (ELISA) kits (Fig. 1K and L). The ELISA results indicated that the DHCNPs showed strong TNF-α- and IL-1β-scavenging abilities in a concentration-dependent manner and had a half-maximal inhibitory concentration (IC50) value of 180.3 μg mL^{-1} for TNF-α and 319.6 μg mL^{-1} for IL-1β, respectively.

3.2. Specific lesion targeting effect of DHCNPs

Since neutrophil infiltration plays a central role in neuroinflammation, targeting inflammatory neutrophils is a novel strategy to treat neuroinflammation. In the acute ischemic stroke mouse model, we have demonstrated that P-selectin that expressed on platelet membranes could specifically target inflammatory neutrophils [29]. Given that high binding affinity can be achieved through the interaction of P-selectin on platelets and P-selectin glycoprotein ligand-1 (PSGL-1) on neutrophils

[43]. Thus, we wondered that the DHCNPs, which have platelet membranes on the surface, could also hijack neutrophils to arrive at the injured spinal cord. First, a cell viability assay was performed, the results indicated that the effects of DHCNPs on neutrophils were negligible (Fig. S4), demonstrating good biocompatibility of DHCNPs. Next, to investigate the self-recognition capability of DHCNPs for neutrophil hijacking, we administered various FITC-labeled nanoparticles to SCI mice. After 1 h, peripheral blood neutrophils of the treated mice were isolated and visualized using confocal laser scanning microscopy (CLSM) (Fig. 2A). Resulting images showed that the DHCNP group exhibited stronger green fluorescence compared with the CL group, demonstrating the neutrophils targeting ability of DHCNPs. In accordance with CLSM images, flow cytometry analysis results also showed that the DHCNPs group had the highest fluorescence intensity, which was about 2.6-fold higher than that of the CLs group (Fig. S5). The above results indicated that DHCNPs could selectively target to circulating neutrophils, which is a critical step for successful injured spinal cord-targeted delivery.

To investigate the ability of DHCNPs to target the SCI site, *in vivo* imaging and two-photon imaging were studies. To visualize DHCNPs *in vivo*, the liposome cores were labeled with DiR or Rhodamine B (RhB). Then, DiR-labeled DHCNPs were intravenously injected into the SCI mice, the *in vivo* fluorescence images showed that the fluorescence signal of DiR was observed in the lesion area and gradually increased over time and reached the maximum at 4 h after injection, then decreased during the following 8 h (Fig. 2B). The results were confirmed by the quantitative region-of-interest (ROI) analysis, DHCNPs showed 1.8-fold and 3.0-fold higher fluorescence intensity than that of DiR-CLs and free DiR, respectively (Fig. 2C). Next, the DiR-CL- and DiR-DHCNP-treated mice were sacrificed and main organs and spinal cords were taken out for *ex vivo* imaging (Fig. 2D). The results indicated that both DiR-CLs and DiR-DHCNPs were mainly distributed in the liver, lung, kidney, and spinal cord after injection, and their fluorescence signals were attenuated as time extended. The quantitative analysis showed that DiR-DHCNPs distribution rate in the spinal cord was significantly higher than that of DiR-CLs (Fig. S6). For further quantitative detection, the Cur concentration in different tissues was examined by HPLC analysis (Fig. S7). The Cur concentration in the spinal cord of the DHCNPs group was significantly higher than that of CLs group at different time points after administration, in good agreement with the fluorescence imaging results. It was worth noting that DHCNPs also had relatively high accumulation in the liver and lung. However, the peak distribution of DHCNPs in the liver is slightly delayed, which may be attributed to the coating of the hybrid cell membranes, extending the circulation time of the DHCNPs (Fig. S8 and Table S2). The above *in vivo* and *ex vivo* drug distribution results demonstrated that the hybrid membrane of the DHCNPs could significantly enhance their spinal cord targeting ability.

It is well established that *in vivo* optical imaging of the spinal cord provide dynamic information about microvessels located in the deep grey matter of living mice [36]. To further demonstrate spinal cord targeting of DHCNPs, a high-speed imaging technique for two-photon imaging was used to visualize the accumulation of RhB-labeled DHCNPs in spinal cord vascular lesions 4 h after administration in living mice (Fig. 2E). Under real-time imaging, the DHCNPs (red) were successfully positioned at lesion area around microvessels (green), while this phenomenon could hardly be observed in the RhB-labeled CLs group. In addition, immunofluorescence images of spinal cord sections showed that DHCNPs and neutrophils colocalized well in the injured region (Fig. S9), which further verified the superior neutrophil targeting specificity of DHCNPs. These results demonstrated that the DHCNPs could hijack neutrophils and travel across BSCB to the injured spinal cord.

3.3. DHCNPs improve functional recovery in mice after SCI

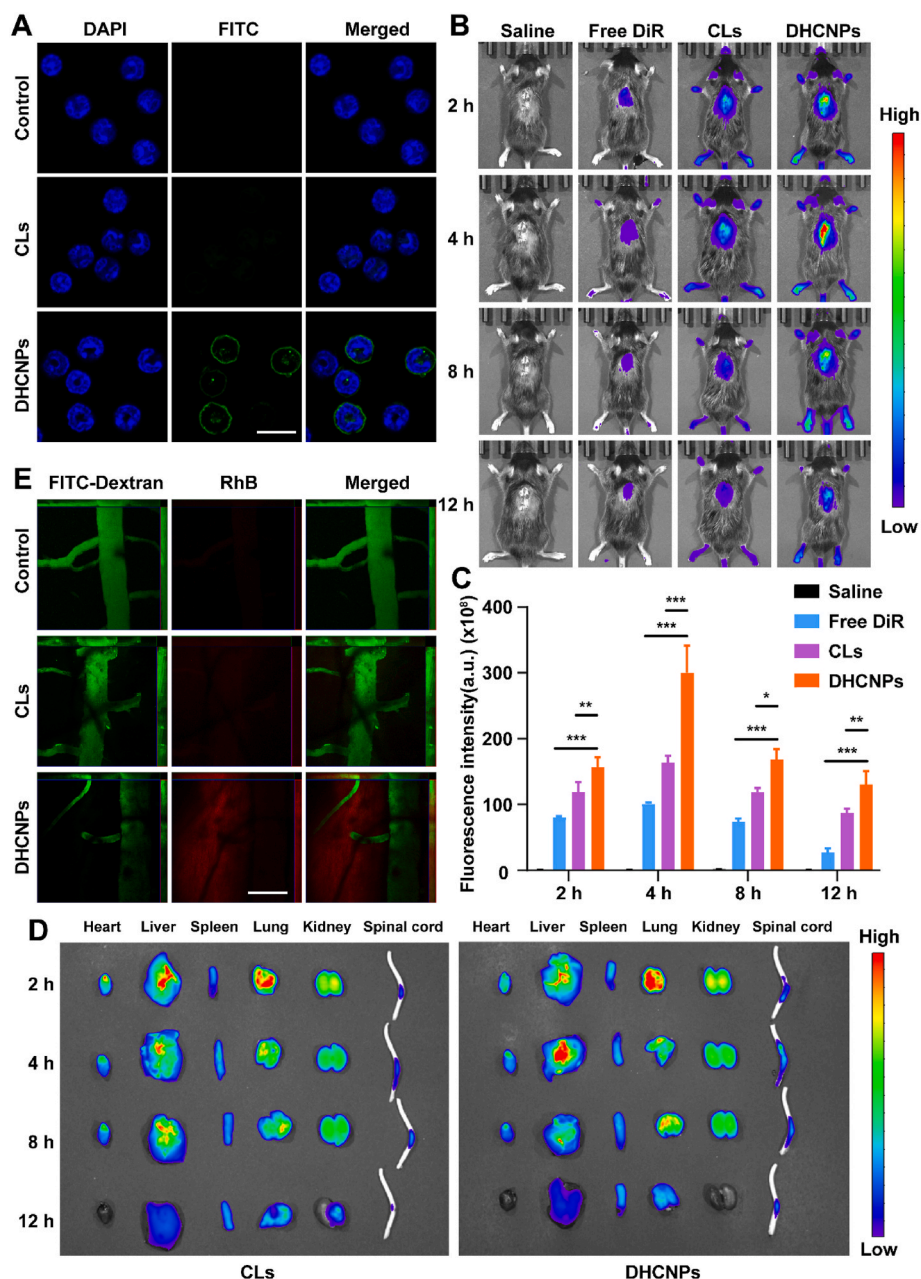After establishing the spinal cord contusion mouse model, saline,

Fig. 2. Specific neutrophils recognition capability and spinal cord injury-targeting effect of DHCNPs. (A) Fluorescence confocal microscopy of neutrophils isolated from SCI mice after the injection of FITC-labeled DHCNPs or FITC-labeled CLs (green), respectively (n = 3). The nucleus was stained by DAPI (blue). The mice injected with saline were used as control group. Scale bar: 10 μm. (B) *In vivo* fluorescence imaging of the SCI mice at 2, 4, 8, and 12 h after intravenous injection of saline, free DiR, DiR-labeled CLs, and DiR-labeled DHCNPs at a DiR dose of 20 nmol/kg (n = 3). (C) ROI analysis of fluorescent intensities from spinal cord area at four time points (n = 3). $*P < 0.05$, $**P < 0.01$, $***P < 0.001$. (D) *Ex vivo* fluorescence imaging of the excised spinal cord and major organs treated with DiR-labeled CLs and DiR-labeled DHCNPs at four time points. (E) Intravital images of spinal cord of SCI mice after injected RhB-labeled CLs and RhB-labeled DHCNPs (red). Blood vessels (green) were labeled by intravenous injection of FITC-dextran (MW = 2000 KDa). The mice injected with saline were used as control group. Scale bar: 200 μm.

HCNPs (without conjugated DNAse I), DHNPs (without loading Cur), and DHCNPs were intravenously administered for three time points at 1, 12, and 24 h, and the motor capacity of the hindlimb was recorded (Fig. 3A). The Basso mouse scale (BMS) scoring system was used to assess the recovery of locomotor functions of SCI mice (Fig. 3B). All the mice exhibited normal open field locomotion before SCI (BMS score = 9) and showed complete hindlimb paralysis at 1 d postinjury (BMS score = 0). Compared with saline group, all the treatment groups showed significantly increased BMS score at the early stage from day 3 after SCI, which was also consistent with the observations on the spinal cord tissues. The gross morphology of the lesion site was clear after SCI and the lesion area was notably smaller after treatment with DHCNPs (Fig. 3C).

Besides, the BMS score of the DHCNP-treated mice was highest among all the groups at 28 d postinjury, indicating that early treatment of DHCNPs could significantly promote the locomotor recovery. It is noteworthy that delivering DHCNPs into the spinal cord at the late stage of SCI (3, 5, 7 d after SCI) failed to ameliorate hindlimb function (Fig. S10). Since the early/acute phase of neuroinflammation was undesirable, whereas the late/chronic phase may have beneficial roles [12, 13], the influence of DHCNPs on the neurological recovery in the late chronic phase of SCI was further studied. Histological examinations were used to evaluate the tissue repair effect of DHCNPs in the late chronic phase. Luxol fast blue (LFB) and immunofluorescence staining results showed that the DHCNPs-treated mice exhibited less
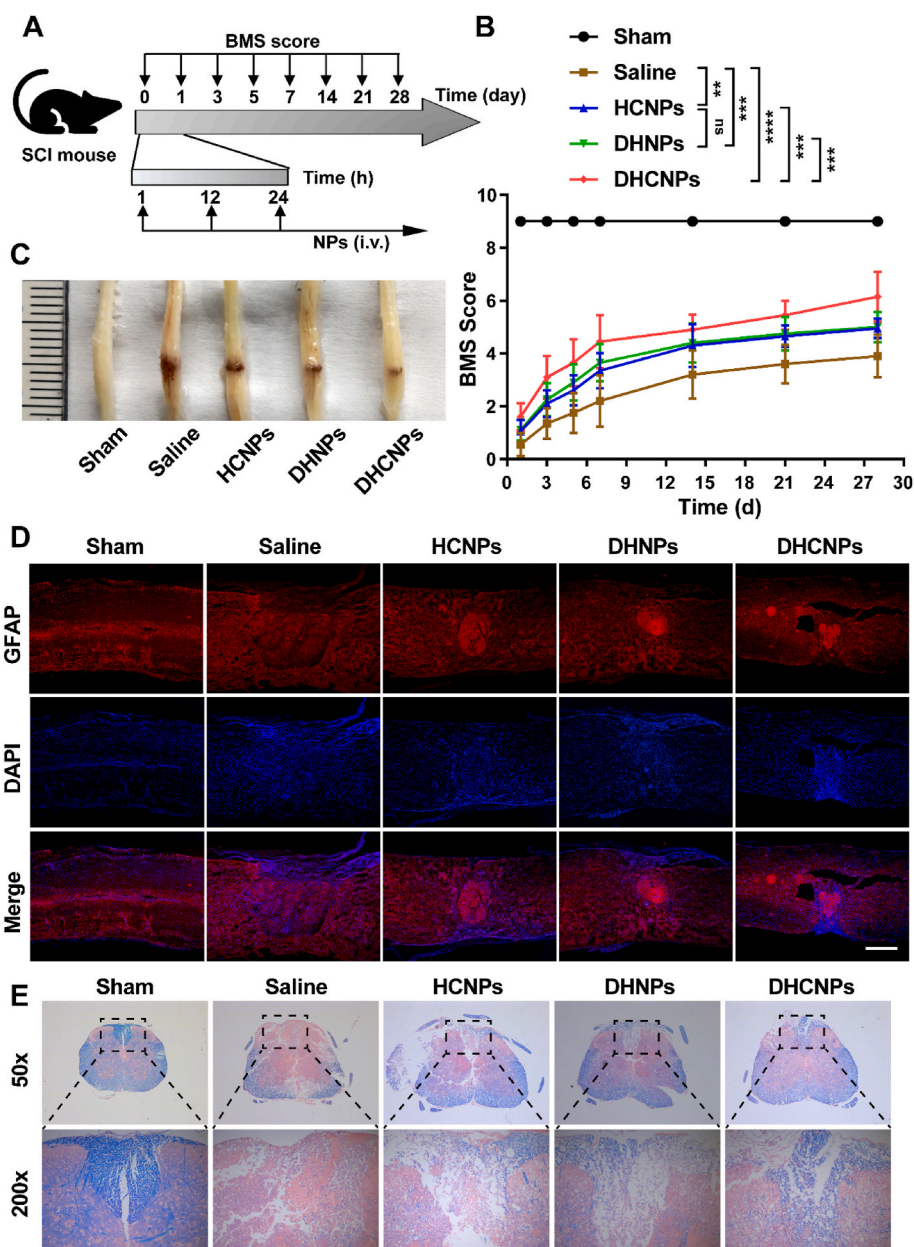
Fig. 3. SCI therapeutic effects of DHCNPs. (A) The study protocol of a treatment process with SCI mouse model. (B) BMS scores of mice in various groups at different time points (n = 10). **$P < 0.01$, ***$P < 0.001$, ****$P < 0.0001$. (C) Representative photo of the spinal cord collected from SCI mice at 3 days after different treatments. (D) Confocal fluorescence images of GFAP (red) in injured spinal cord of each group at 28 d postinjury. The nucleus was stained by DAPI (blue). Scale bar: 500 μm. (E) LFB staining of the injured spinal cords (transverse sections). Low magnification images are on the top (50 ×), and higher magnification images of the boxed regions are on the bottom (200 ×).

demyelination and cavity formation and better tissue preservation (Fig. 3D and E). However, no obvious differences were observed among other groups, demonstrated Cur loading and DNAse I conjugation could attenuate locomotor impairment, while their combination could promote function recovery after SCI.

3.4. DHCNPs degrade neutrophil extracellular traps after SCI

It is recognized that neutrophils are the key effector cells in the pathogenesis of SCI. Additionally, excessive infiltrating neutrophils in the acute phase of SCI could induce NETs formation, known as NETosis. The generated NETs potentiate a potent inflammatory process by triggering the release of "damage-associated molecular pattern (DAMP)", impair revascularization and vascular remodeling, and cause the

apoptosis or necrosis of neuronal cells. Therefore, restricting NETs is potentially clinically applicable biointervention for reversing SCI [44]. Given that NETs can injure host tissues, we next studied the ability of DHCNPs to digest NETs generated by neutrophils. First, we mimicked the NETs degradation process in response to DHCNPs treatment *in vitro* for detailed investigation. NETs were induced by the stimulation of neutrophils with phorbol 12-myristate 13-acetate (PMA, a strong stimulator of NET formation) [39], which resulted in increased release of granular proteins and chromatin in a DNA framework compared with unstimulated neutrophils (Fig. S11). Then, the successful establishment of DNA web-like NETs were incubated with DHCNPs. As expected, DHCNPs significantly degraded the formed NETs compared with the vehicle controls (Fig. S12).

To further evaluate the DHCNPs could degrade NETs after injury *in*

vivo, we performed western blot analysis of a specific marker (i.e., citrullinated histone H3 (H3Cit)) of NETs formation in the injured spinal cord at 24 h after DHNPs and DHCNPs treatment. The results showed that the amounts of H3Cit in the injured spinal cord were largely reduced after DHNPs and DHCNPs treatment (Fig. 4A and B). Similarly, examination of the plasma revealed that DHNPs and DHCNPs treatments both decreased the levels of circulating DNA (Fig. 4C). Immunostaining results revealed that the injured site was extensively labeled with H3Cit+ cells at 24 h. To identify which type of cells expressed H3Cit after injury, double immunofluorescence staining of spinal cord sections was performed. The results revealed that the red H3Cit signal was mostly colocalized with Ly6G+ neutrophils and the ratio of H3Cit+ neutrophils were significantly decreased in DNAse I-modified groups (i.e., DHNPs and DHCNPs groups), whereas the treatment with HCNPs had no visible down-regulatory effect (Fig. 4D and E). To confirm these observations, we further identified NETs degradation using *in vivo* multiphoton microscopic imaging of extracellular DNA via intravenously administered Sytox green. The results revealed that DHNPs and DHCNPs significantly reduced Sytox green-positive extracellular DNA fibers in the injured spinal cord, whereas these fibers abundantly detected in control groups (Fig. 4F and G). Together, our data indicated that DHCNPs could effectively degrade NETs, thereby potentially inhibit neuroinflammation and increase revascularization and neurorestoration.

3.5. DHCNPs inhibit NF-κB pathway and reverse the proinflammatory microenvironment after SCI

Neuroinflammation, on the other hand, refers to the inflammatory response within the brain or spinal cord, triggered by various noxious stimuli. This inflammatory process involves the activation of resident immune cells and the production of cytokines, chemokines, and ROS, which can lead to tissue damage and neuronal dysfunction. Accumulating evidence suggests neuroinflammation and NETs are intricately linked, with NETs playing a significant role in amplifying and perpetuating neuroinflammatory responses [15,22]. However, the underlying primary signaling mechanisms that govern the influence of NETs on neuroinflammation remain largely unmapped. Nuclear factor kappa B
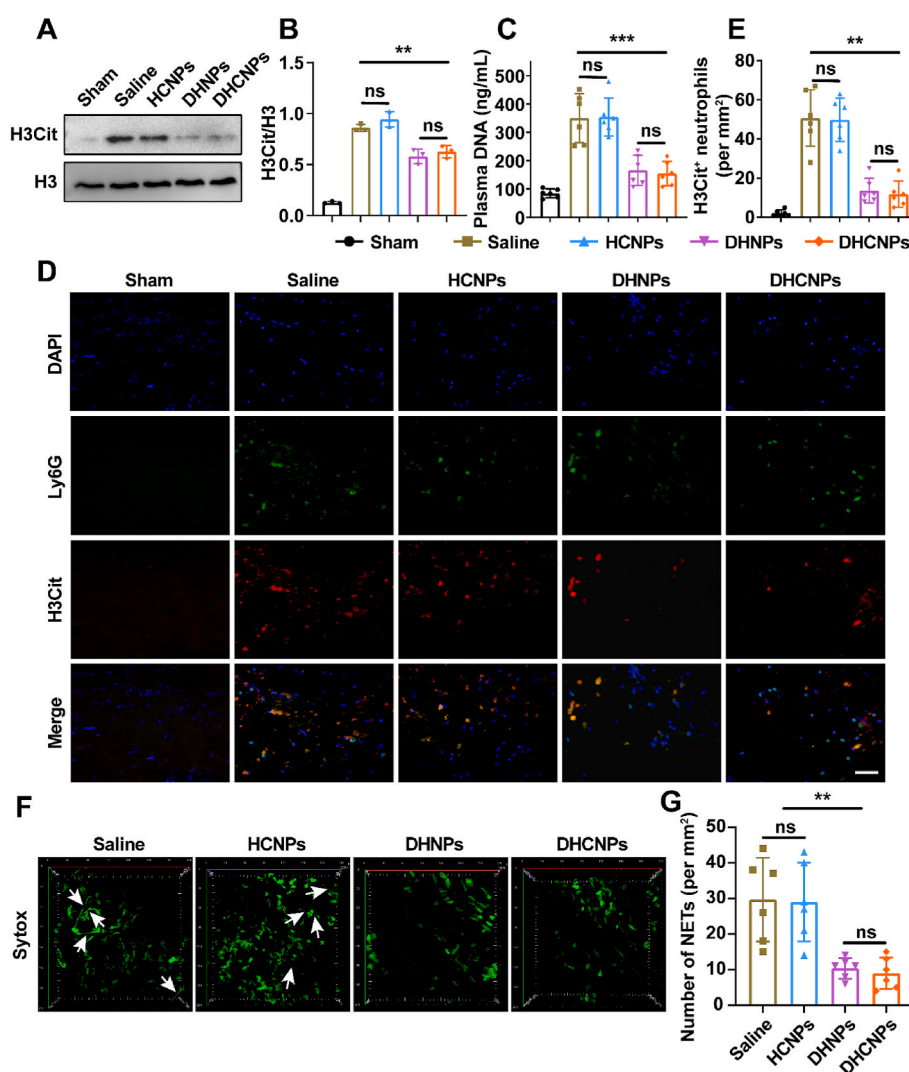

Fig. 4. DHCNPs digested NETs presenting in the spinal cord after SCI. (A, B) Representative immunoblots and quantification of H3Cit levels in the spinal cord of SCI mice treated with Saline, HCNPs, DHNPs, or DHCNPs at 24 h postinjury. Sham mice were used as controls (n = 3). **$P < 0.01$. (C) The levels of plasma DNA of each group at 24 h postinjury (n = 6). ***$P < 0.001$. (D) Representative confocal images of neutrophil (Ly6G, green) and H3Cit (red) immunostaining in spinal cord of each group at 24 h postinjury. Sham mice were used as controls. The nucleus was stained by DAPI (blue). Scale bar: 50 μm. (E) Quantification of the numbers of H3Cit-positive neutrophils in the spinal cord 24 h in SCI mice treated with Saline, HCNPs, DHNPs, or DHCNPs (n = 6). **$P < 0.01$. (F) *In vivo* multiphoton microscopic images of extracellular DNA (Sytox, green) in spinal cord of SCI mice treated with Saline, HCNPs, DHNPs or DHCNPs at 24 h postinjury. Arrows indicate extracellular DNA fibers. (G) Quantification of NETs for each group (n = 6). **$P < 0.01$.

(NF-κB) is a well-established player in biological processes, particularly inflammation. Notably, a BALB/c mouse model, designated as the NF-κB-RE-luc mouse, has been instrumental in investigating NF-κB activation *in vivo*. When exposed to various stimuli, including inflammatory responses in SCI, NF-κB activation in the NF-κB-RE-luc mouse triggers an upregulation of luciferase expression (Fig. 5A). Notably, as illustrated in Fig. 5B, administration of DHCNPs significantly inhibited NF-κB activation induced by SCI, as evidenced by a marked decrease in IVIS signal intensity (Fig. 5C). NF-κB activation involves three stages: proinflammatory signals activate the IκB kinase (IKK) complex (IKKα,

IKKβ, and IKKγ), leading to IκB degradation, particularly IκBα. This prompts the rapid release of NF-κB dimers (e.g., p65/p50) into the nucleus, triggering proinflammatory gene transcription [45,46]. As expected, following DHCNPs treatment, a significant reduction in the expression of p-IκBα and p-p65, along with a corresponding increase in IκBα level, was observed. However, there was no significant difference in the total protein level of p65. (Fig. 5D–E). It is worth noting that the HCNPs group loaded solely with curcumin also suppressed the activation of IKK, preventing the phosphorylation and subsequent degradation of IκB proteins. This result indicates that curcumin has an inhibitory
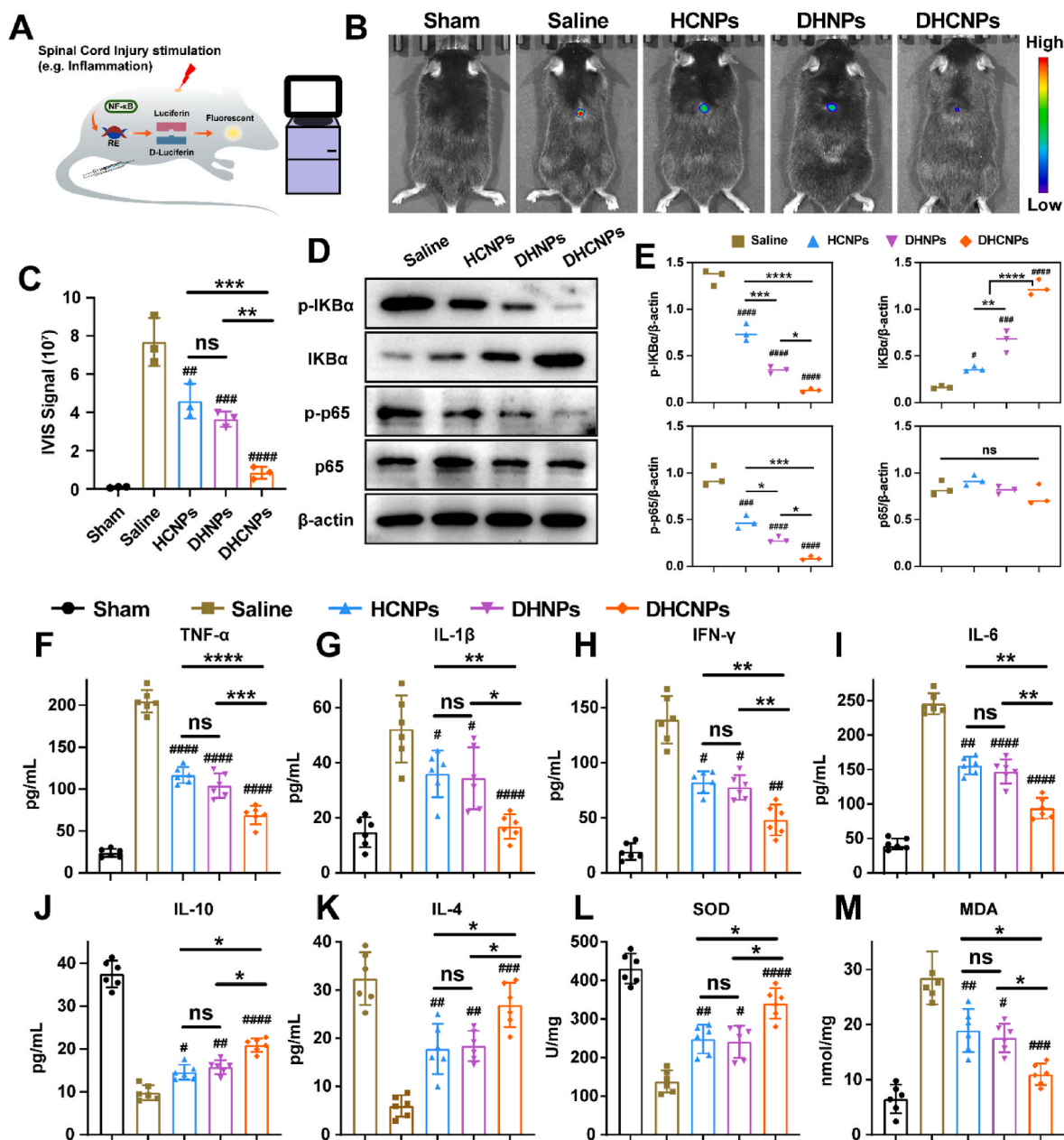

Fig. 5. DHCNPs inhibited the NF-κB pathway, mitigating neuroinflammation. (A) A schematic of the NF-κB-RE-luc mouse SCI model shows NF-κB binding to response elements (RE) upon inflammatory stimuli, activating luciferin expression and fluorescence emission upon D-luciferin injection. (B, C) Representative bioluminescence images (B) and IVIS signal (C) depicting NF-κB activation in NF-κB-RE-luc mice following various treatments (D–F) Representative immunoblots (D) and quantification results of p-IκBα, IκBα, p-p65 and p65 (E) with different treatments (n = 3). One-way ANOVA (*P < 0.05, **P < 0.01, ***P < 0.001, ****P < 0.0001) was used to identify significant differences between the treatment groups. Statistical significance between the labeled groups and the saline group: #P < 0.05, ##P < 0.01, ###P < 0.001, ####P < 0.0001. (F–K) The expression levels of proinflammatory cytokines TNF-α, IL-1β, IFN-γ, IL-6, IL-10, and IL-4 in the spinal cord at 24 h postinjury. (L, M) The concentration of SOD and MDA in spinal cord tissue at 24 h postinjury (n = 6). One-way ANOVA (*P < 0.05, **P < 0.01, ***P < 0.001, ****P < 0.0001) was used to identify significant differences between the treatment groups. Statistical significance between the labeled groups and the saline group: #P < 0.05, ##P < 0.01, ###P < 0.001, ####P < 0.0001.

effect on NF-kB activation, consistent with previous literature reports [47].

It has long been recognized that pro-inflammatory M1 microglia are the primary effector cells of inflammatory responses following SCI, promoting the release of inflammatory factors and ROS, ultimately causing inflammatory damage to tissues [48]. To investigate whether DHCNPs influence the polarization of M1 microglia, spinal microglia were stained with M1-related surface markers and analyzed using flow
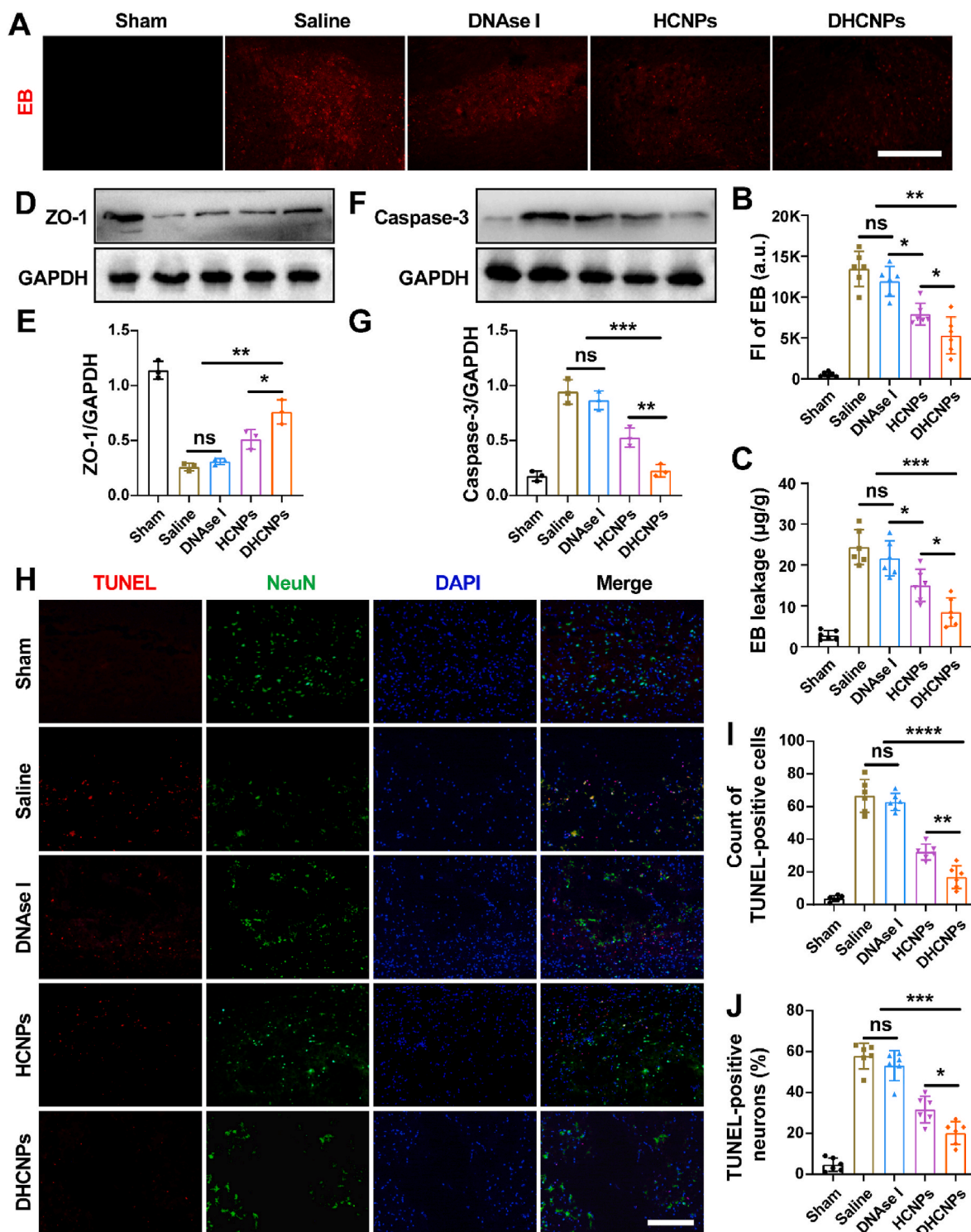

Fig. 6. DHCNPs promoted BSCB restoration and nerve repair. (A) Representative fluorescence images of EB (red) leakage at the injury epicenter of SCI mice treated with Saline, DNAse I, HCNPs, or DHCNPs at 24 h postinjury. Sham mice were used as control. Scale bar: 500 μm. (B, C) Fluorescence intensity of EB and Quantification of EB leakage at the injury epicenter of each group (n = 6). *P < 0.05, **P < 0.01, ***P < 0.001. (D–G) Representative immunoblots and quantification results of ZO-1 and caspase-3 in the injured spinal cord of each group at 24 h postinjury. Sham mice were used as control (n = 3). *P < 0.05, **P < 0.01, ***P < 0.001. (H) Representative confocal fluorescence images of TUNEL (red)- and NeuN (green)-stained tissues in the spinal cord of each group at 24 h postinjury. Sham mice were used as control. Before imaging, the nuclei were stained by DAPI (blue). Scale bar: 200 μm. (I, J) Quantification of the numbers of TUNEL-positive cells and double-positive cells in injured spinal cord of each group (n = 6). *P < 0.05, **P < 0.01, ***P < 0.001, ****P < 0.0001.

cytometry. Our findings revealed a significant increase in the percentage of CD11c-expressing spinal microglia (M1 marker) in SCI mice. Notably, when compared to other groups, the expression of CD11c was significantly decreased in the DHCNPs group, indicating a potential inhibitory effect of DHCNPs on M1 microglia polarization (Fig. S13). To further evaluate the anti-inflammatory effect of DHCNPs, we determined the levels of inflammation-related cytokines (e.g., TNF-α, IL-1β, IFN-γ, IL-6, IL-10, and IL-4), SOD, MDA, and MPO in the spinal cords of SCI mice at 24 h postinjury in different groups. In all drug-treated groups, local pro-inflammatory cytokines, including TNF-α, IL-1β, IFN-γ, and IL-6 were downregulated, while anti-inflammatory cytokines, including IL-10 and IL-4 were up-regulated. The levels of pro-inflammatory cytokines and anti-inflammatory cytokines were significantly lower and higher in the DHCNPs group than in the HCNPs and DHNPs groups, respectively (Fig. 5F–M). Then, the MDA, MPO, and SOD levels were studied to evaluate the antioxidant effect of DHCNPs. The MDA and MPO levels in the treatment groups were decreased and the SOD level was increased than in the saline group. In addition, the levels of all three cytokines in the DHCNPs group were closest to those in the sham groups (Fig. 5L and M and S14). These results suggested that DHCNPs efficiently blocked the NF-κB inflammatory signaling pathway, consequently mitigating the expression of pro-inflammatory genes and suppressing the inflammatory response.

3.6. DHCNPs enhance BSCB restoration and protect neurons after SCI

Endothelial cells and neurons serve as the fundamental structural and functional components of the nervous system, playing a pivotal role in determining the prognosis of SCI [49]. Given the exceptional NETs digesting ability of DHCNPs, which effectively inhibits the NF-κB pathway and alleviates neuroinflammation, we further examined whether these nanoparticles could enhance BSCB restoration and safeguard neurons from degradation caused by NETs. We used evans blue (EB) to measure vascular permeability in spinal cord. Both EB fluorescence and EB leakage results indicated that BSCB disruption was significantly ameliorated at 24 h postinjury in the DHCNPs group, whereas treatment with free DNAse I had negligible ameliorating effect, probably owing to its poor stability or short systemic circulation time (Fig. 6A–C). It is noteworthy that the HCNPs group could also reduce EB leakage to some extent, mainly due to the anti-inflammatory effect of the loaded drug Cur and the role of neutralizing inflammatory factors in the fusion membrane. Moreover, the expression of tight junction protein zona occludens-1 (ZO-1) that maintain the integrity of the BSCB is reduced after SCI. However, the expression of these two kinds of proteins were not reduced after DHCNPs treatment (Fig. 6D and E), further demonstrating that BSCB disruption of SCI mice was inhibited after administration of DHCNPs.

Since NETs have a destructive impact on spinal neurons and have been detected in the lesion of injured spinal cord, we further evaluated whether DHCNPs could protect neuron after SCI. First, we mimicked the process of NETs interfering neurons *in vitro* and evaluated the survival of interfered neurons in response to DHCNPs treatment. As expected, co-culturing primary spinal cord neurons with NETs significantly aggravated neuronal death, while DHCNPs dramatically enhanced neuronal survival via degrading NETs (Fig. S15). On the other hand, caspase-3 is a key enzyme of cell apoptosis and mediate cell death of neurons [50]. Thus, the expression of caspase-3 in the injured spinal cord after injection of different formulations was explored. Compared with other groups, the expression of caspase-3 at 24 h postinjury decreased significantly in the DHCNPs group (Fig. 6F and G). Furthermore, double immunofluorescence staining of neuron-specific nuclear protein (NeuN) and TdT-mediated dUTP-biotin nick end labeling (TUNEL) also indicated that DHCNPs exhibited minimal neuron death at the epicenter of lesion after SCI (Fig. 6H–J). These results demonstrated that DHCNPs could promote BSCB and nerve repair by restricting NETs.

3.7. Biocompatibility and toxicity evaluation of DHCNPs

In vivo biosafety is always a considerable concern in the field of nanomaterials. To evaluate the biocompatibility of DHCNPs, mice were weighed and sacrificed at the end of the treatment, and major organs and blood were collected for hematoxylin and eosin (H&E) histological and hematological analysis. As expected, no obvious pathological change was found in the main organs of all the groups, indicating the good biocompatibility of the used nanomaterials (Fig. 7A). In addition, no difference in the body weight, blood hematology, and biochemistry analysis was observed among different groups at 28 days postinjury (Fig. 7B). The above results showed that DHCNPs had satisfactory biocompatibility, suggesting promise for clinical application.

4. Discussion

Traumatic SCI is a devastating condition that leads to severe neurological deficits and permanent damage. The pathophysiology of SCI involves both a primary injury, resulting from the initial mechanical trauma, and a secondary injury cascade that is characterized by neuroinflammation [1,5]. Among the various inflammatory responses, the role of neutrophils and their extracellular traps (NETs) has emerged as a crucial factor in exacerbating SCI. NETs are web-like structures released by activated neutrophils, composed primarily of DNA fibers decorated with histones and granular proteins [15]. While NETs serve an important role in host defense against pathogens, their excessive or dysregulated production during SCI can have detrimental effects. NETs have been shown to promote inflammation by activating immune cells and releasing pro-inflammatory cytokines and chemokines. In addition, NETs can cause vascular occlusion, impairing blood flow to the injured spinal cord and further aggravating tissue damage [22]. Importantly, NETs have been implicated in disrupting the BSCB, which normally functions to protect the spinal cord from harmful substances in the blood. The disruption of the BSCB allows for the infiltration of immune cells and inflammatory mediators into the spinal cord parenchyma, further amplifying the inflammatory response and causing neuronal damage [17,20].

NF-κB signaling pathway is a central regulator of inflammation, cell survival, and apoptosis. Upon activation by various stimuli such as cytokines, reactive oxygen species, and cellular stress, NF-κB translocates to the nucleus and activates the transcription of genes involved in these biological processes [45]. In the context of SCI, NF-κB activation leads to the production of pro-inflammatory cytokines and chemokines, which exacerbate tissue damage and promote cell death. The interplay between NF-κB signaling pathway and NETs in SCI is complex and multifaceted [51–53]. On one hand, NF-κB activation can promote the production of cytokines and chemokines that further activate neutrophils, leading to the release of NETs. These NETs, in turn, can activate NF-κB in a positive feedback loop, amplifying the inflammatory response. On the other hand, NETs themselves can activate NF-κB signaling pathway directly, leading to the production of additional pro-inflammatory mediators [45,46]. The interaction between NF-κB and NETs provides potential therapeutic targets for SCI. By inhibiting NF-κB activation, one can reduce the production of pro-inflammatory mediators and mitigate the inflammatory response. This, in turn, can lead to reduced NETs formation and decreased tissue damage. Conversely, targeting and degrading NETs can also mitigate NF-κB activation, further reducing inflammation and promoting tissue repair.

DNase I, a naturally occurring plasma endonuclease, has garnered significant attention as a potential therapeutic for degrading neutrophil extracellular traps (NETs). Nevertheless, its clinical application has been stymied by several limitations, including poor stability, a short half-life, low bioavailability, and inadequate penetration capabilities [54]. Furthermore, systemic administration of DNase I often requires high doses, which can lead to unwanted side effects such as the formation of anti-DNase antibodies [55]. To overcome these hurdles and enhance its
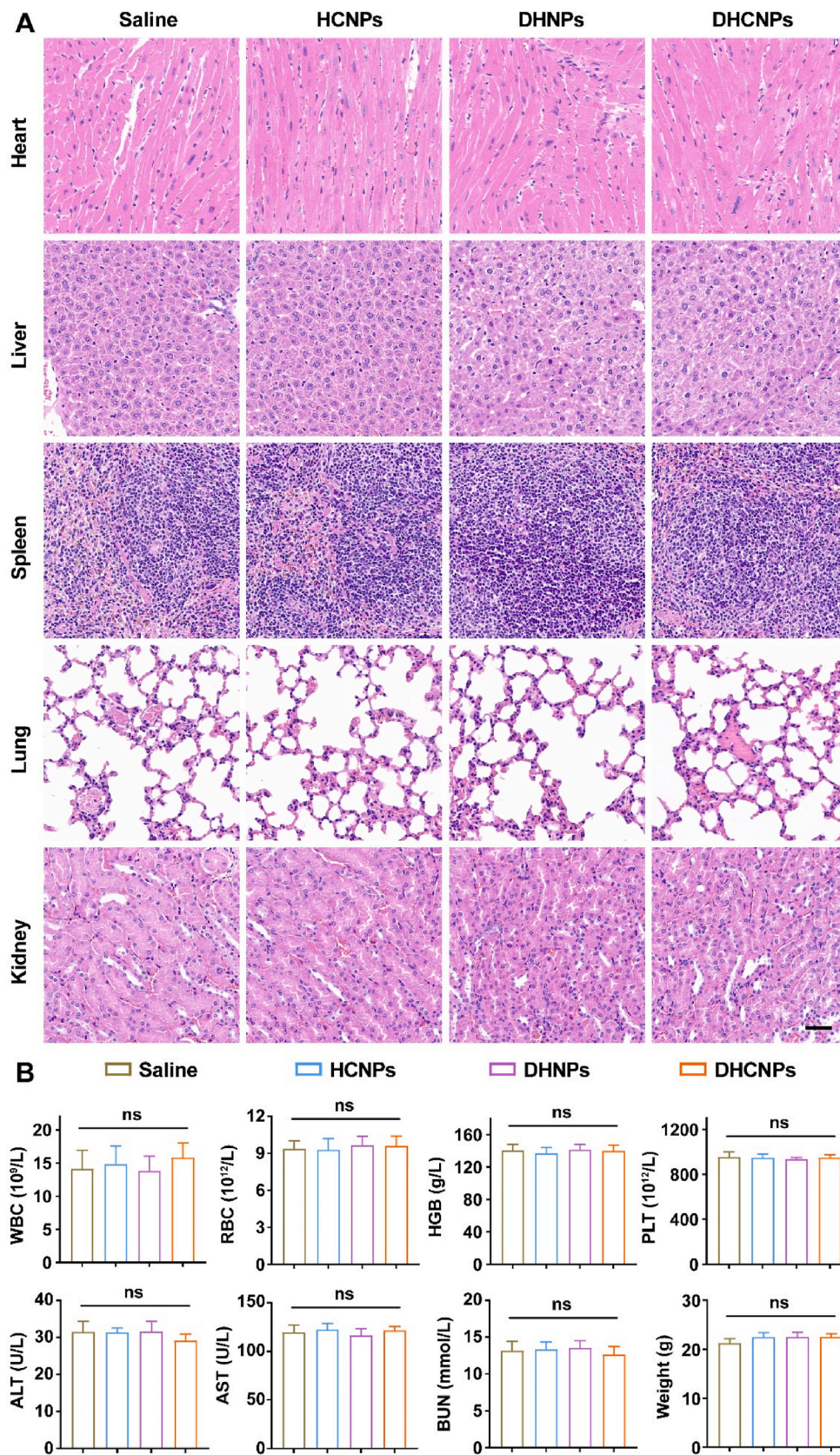
Fig. 7. *In vivo* toxicity evaluation of DHCNPs. (A) H&E staining of main organs including heart, liver, spleen, lung, and kidney separated from SCI mice intravenously injected with saline, HCNPs, DHNPs, or DHCNPs at the indicated time points (1, 12, and 24 h). Scale bar: 50 μm. (B) Hematological analysis and body weight of mice of each group at 28 days postinjury. WBC, white blood cells; RBC, red blood cells; HGB, hemoglobin; PLT, platelets; ALT, alanine transaminase; AST, aspartate transaminase; BUN, blood urea nitrogen (n = 6).

therapeutic efficacy, nanocarrier-mediated delivery of DNase I has emerged as a promising solution. While previous studies successfully prolonged DNase I's plasma half-life, they fell short in imparting active targeting abilities necessary for effective accumulation at sites of inflammation. Additionally, direct encapsulation within liposomes was found to hinder DNase I's catalytic efficiency due to the presence of lipid bilayer barriers [56]. Consequently, there remains a pressing need to develop a DNase I delivery system that combines active targeting, biocompatibility, and high enzymatic activity.

Addressing the challenges associated with traditional DNase I delivery, researchers have crafted innovative strategies that harness the potential of targeted nanoparticles conjugated with this enzyme. Nina Filipczak et al. for instance, pioneered a nanopreparation featuring nucleosome-targeted antibody 2C5-functionalized micelles coated with DNase I, enabling specific recognition and degradation of NETs [25]. Likewise, Yang Du et al. introduced a groundbreaking biomimetic DNase I delivery system employing genetically and bioorthogonally engineered cellular nanovesicles, showcasing remarkable NETs clearance in acute lung injury models [57]. Building upon these pioneering efforts, our study presents DHCNPs, a novel biomimetic nanoplatform tailored to target and degrade NETs, thereby modulating the neuroinflammatory microenvironment and fostering spinal cord injury (SCI) recovery.

The strengths of our approach are manifold. By incorporating curcumin, a renowned anti-inflammatory agent, within the liposome core and adorning the hybrid membrane with DNase I, we achieve concurrent targeting of diverse neuroinflammatory aspects. This holistic strategy promises enhanced therapeutic efficacy over single-target interventions. Moreover, the utilization of biomimetic membranes, which seamlessly fuse platelet and neutrophil membranes, not only reinforces biocompatibility and targeting precision but also facilitates the hijacking of neutrophils and neutralization of proinflammatory cytokines, further amplifying the therapeutic prowess of DHCNPs. *In vivo* investigations underscored the remarkable therapeutic potential of DHCNPs. Motor function tests revealed significant improvements in functional recovery post-SCI. Histological examinations illuminated their ability to mitigate tissue damage, reduce demyelination and cavity formation, while preserving neuronal architectures. These salutary effects stem from DHCNPs' capacity to degrade NETs, quell neuroinflammation, and facilitate BSCB restoration.

While the clinical translation of our nanoplatform holds significant promise for SCI treatment, offering a potentially safer and more effective option compared to current standard therapies, several challenges must be addressed. These include optimizing the formulation for stability and shelf-life, ensuring scalability for manufacturing, and conducting rigorous preclinical safety and efficacy studies. Additionally, navigating the regulatory pathway for such a novel therapeutic approach, including obtaining necessary approvals for human trials, is essential. Despite these challenges, the potential impact of DHCNPs on improving the lives of SCI patients underscores the importance and worthiness of pursuing their clinical translation.

5. Conclusion

In summary, we reported a multi-targeted bioinspired nanotherapeutics (DHCNPs) for modulating the complicated neuroinflammatory microenvironment at an early stage of SCI. Notably, the DHCNPs could hijack inflammatory neutrophil as potential molecular Trojan horses for BSCB penetration and increase the injured spinal cord accumulation. Owing to the injured spinal cord targeting ability, DHCNPs efficiently neutralized proinflammatory cytokines, digested NETs generated by neutrophils in the injured area, promoted BSCB restoration and nerve repair, and relieved oxidative stress to promote neuron survival. Thus, DHCNPs created a microenvironment suitable for neural regeneration and eventually promoted neurological functional recovery through modulating the NF-κB pathway. Therefore, this biomimetic multi-target nanodrug platform helps to explore the possibilities of rescuing SCI at an early stage by focusing on normalizing overwhelming neuroinflammatory microenvironment, and it offers broad potential applications for other neuroinflammatory disorders.

Availability of data and materials

Data will be made available on request.

CRediT authorship contribution statement

Chunming Tang: Writing – original draft, Investigation, Funding acquisition, Formal analysis, Conceptualization. **Yaoyao Jin:** Writing – original draft, Data curation. **Min Wu:** Writing – original draft, Validation, Data curation. **Feng Jia:** Writing – original draft. **Xiaowei Lu:** Validation, Formal analysis. **Jinyu Li:** Formal analysis, Data curation. **Jie Wu:** Formal analysis, Data curation. **Senlin Zhu:** Visualization, Validation, Software. **Zhiji Wang:** Visualization, Validation, Software. **Di An:** Visualization, Validation, Software. **Wu Xiong:** Validation, Resources, Methodology. **Yongjie Zhang:** Writing – review & editing, Validation, Supervision, Resources. **Huae Xu:** Writing – review & editing, Validation, Supervision, Funding acquisition. **Xufeng Chen:** Writing – review & editing, Supervision.

Declaration of competing interest

The authors declare that they have no known competing financial interests or personal relationships that could have appeared to influence the work reported in this paper.

Data availability

Data will be made available on request.

Acknowledgements

Appendix A. Supplementary data

Supplementary data to this article can be found online at https://doi.org/10.1016/j.mtbio.2024.101218.

References

[1] I. Eli, D.P. Lerner, Z. Ghogawala, Acute traumatic spinal cord injury, Neurol. Clin. 39 (2) (2021) 471–488.

[2] A. Alizadeh, S.M. Dyck, S. Karimi-Abdolrezaee, Traumatic spinal cord injury: an overview of pathophysiology, models and acute injury mechanisms, Front. Neurol. 10 (2019) 282.

[3] B. Fiani, M.A. Arshad, E.S. Shaikh, A. Baig, M. Farooqui, M.A. Ayub, A. Zafar, S. A. Quadri, Current updates on various treatment approaches in the early management of acute spinal cord injury, Rev. Neurosci. 32 (5) (2021) 513–530.

[4] J. Donovan, S. Kirshblum, Clinical trials in traumatic spinal cord injury, Neurotherapeutics 15 (3) (2018) 654–668.

[5] J.K. Alexander, P.G. Popovich, Neuroinflammation in spinal cord injury: therapeutic targets for neuroprotection and regeneration, Prog. Brain Res. 175 (2009) 125–137.

[6] X. Freyermuth-Trujillo, J.J. Segura-Uribe, H. Salgado-Ceballos, C.E. Orozco-Barrios, A. Coyoy-Salgado, Inflammation: a target for treatment in spinal cord injury, Cells 11 (17) (2022).

[7] D.J. Allison, D.S. Ditor, Immune dysfunction and chronic inflammation following spinal cord injury, Spinal Cord 53 (1) (2015) 14–18.

[8] X. Hu, W. Xu, Y. Ren, Z. Wang, X. He, R. Huang, B. Ma, J. Zhao, R. Zhu, L. Cheng, Spinal cord injury: molecular mechanisms and therapeutic interventions, Signal Transduct. Targeted Ther. 8 (1) (2023) 245.

[9] I. Pineau, S. Lacroix, Proinflammatory cytokine synthesis in the injured mouse spinal cord: multiphasic expression pattern and identification of the cell types involved, J. Comp. Neurol. 500 (2) (2007) 267–285.

[10] M.B. Bracken, W.F. Collins, D.F. Freeman, M.J. Shepard, F.W. Wagner, R.M. Silten, K.G. Hellenbrand, J. Ransohoff, W.E. Hunt, P.L. Perot Jr., et al., Efficacy of methylprednisolone in acute spinal cord injury, JAMA 251 (1) (1984) 45–52.

[11] R.J. Hurlbert, Methylprednisolone for acute spinal cord injury: an inappropriate standard of care, J. Neurosurg. 93 (1 Suppl) (2000) 1–7.

[12] R. Rust, J. Kaiser, Insights into the dual role of inflammation after spinal cord injury, J. Neurosci. 37 (18) (2017) 4658–4660.

[13] S. David, R. Lopez-Vales, V. Wee Yong, Harmful and beneficial effects of inflammation after spinal cord injury: potential therapeutic implications, Handb. Clin. Neurol. 109 (2012) 485–502.

[14] V. Neirinckx, C. Coste, R. Franzen, A. Gothot, B. Rogister, S. Wislet, Neutrophil contribution to spinal cord injury and repair, J. Neuroinflammation 11 (2014) 150.

[15] S. Zivkovic, M. Ayazi, G. Hammel, Y. Ren, For better or for worse: a look into neutrophils in traumatic spinal cord injury, Front. Cell. Neurosci. 15 (2021) 648076.

[16] A. Ahmed, A.A. Patil, D.K. Agrawal, Immunobiology of spinal cord injuries and potential therapeutic approaches, Mol. Cell. Biochem. 441 (1–2) (2018) 181–189.

[17] L. Kang, H. Yu, X. Yang, Y. Zhu, X. Bai, R. Wang, Y. Cao, H. Xu, H. Luo, L. Lu, M. J. Shi, Y. Tian, W. Fan, B.Q. Zhao, Neutrophil extracellular traps released by neutrophils impair revascularization and vascular remodeling after stroke, Nat. Commun. 11 (1) (2020) 2488.

[18] J. Liu, S. Zhang, Y. Jing, W. Zou, Neutrophil extracellular traps in intracerebral hemorrhage: implications for pathogenesis and therapeutic targets, Metab. Brain Dis. 38 (8) (2023) 2505–2520.

[19] A. Nowaczewska-Kuchta, D. Ksiazek-Winiarek, P. Szpakowski, A. Glabinski, The role of neutrophils in multiple sclerosis and ischemic stroke, Brain Sci. 14 (5) (2024).

[20] K. Vaibhav, M. Braun, K. Alverson, H. Khodadadi, A. Kutiyanawalla, A. Ward, C. Banerjee, T. Sparks, A. Malik, M.H. Rashid, M.B. Khan, M.F. Waters, D.C. Hess, A.S. Arbab, J.R. Vender, N. Hoda, B. Baban, K.M. Dhandapani, Neutrophil extracellular traps exacerbate neurological deficits after traumatic brain injury, Sci. Adv. 6 (22) (2020) eaax8847.

[21] A. Shafqat, A. Noor Eddin, G. Adi, M. Al-Rimawi, S. Abdul Rab, M. Abu-Shaar, K. Adi, K. Alkattan, A. Yaqinuddin, Neutrophil extracellular traps in central nervous system pathologies: a mini review, Front. Med. 10 (2023) 1083242.

[22] Z. Feng, L. Min, L. Liang, B. Chen, H. Chen, Y. Zhou, W. Deng, H. Liu, J. Hou, Neutrophil extracellular traps exacerbate secondary injury via promoting neuroinflammation and blood-spinal cord barrier disruption in spinal cord injury, Front. Immunol. 12 (2021) 698249.

[23] D. Suck, DNA recognition by DNase I, J. Mol. Recogn. 7 (2) (1994) 65–70.

[24] L. Laukova, B. Konecna, L. Janovicova, B. Vlkova, P. Celec, Deoxyribonucleases and their applications in biomedicine, Biomolecules 10 (7) (2020).

[25] N. Filipczak, X. Li, G.R. Saawant, S.S.K. Yalamarty, E. Luther, V.P. Torchilin, Antibody-modified DNase I micelles specifically recognize the neutrophil extracellular traps (NETs) and promote their degradation, J. Contr. Release 354 (2023) 109–119.

[26] Q. Mu, K. Yao, M.Z. Syeda, J. Wan, Q. Cheng, Z. You, R. Sun, Y. Zhang, H. Zhang, Y. Lu, Z. Luo, Y. Li, F. Liu, H. Liu, X. Zou, Y. Zhu, K. Peng, C. Huang, X. Chen, L. Tang, Neutrophil targeting platform reduces neutrophil extracellular traps for improved traumatic brain injury and stroke theranostics, Adv. Sci. 11 (21) (2024) e2308719.

[27] N. Rezaei, M. Zadory, S. Babity, S. Marleau, D. Brambilla, Therapeutic applications of nanoparticles targeting neutrophil and extracellular traps, J. Contr. Release 358 (2023) 636–653.

[28] R.H. Fang, A.V. Kroll, W. Gao, L. Zhang, Cell membrane coating nanotechnology, Adv. Mater. 30 (23) (2018) e1706759.

[29] C. Tang, C. Wang, Y. Zhang, L. Xue, Y. Li, C. Ju, C. Zhang, Recognition, intervention, and monitoring of neutrophils in acute ischemic stroke, Nano Lett. 19 (7) (2019) 4470–4477.

[30] Q. Zhang, D. Dehaini, Y. Zhang, J. Zhou, X. Chen, L. Zhang, R.H. Fang, W. Gao, L. Zhang, Neutrophil membrane-coated nanoparticles inhibit synovial inflammation and alleviate joint damage in inflammatory arthritis, Nat. Nanotechnol. 13 (12) (2018) 1182–1190.

[31] G. Gu, J. Ren, B. Zhu, Z. Shi, S. Feng, Z. Wei, Multiple mechanisms of curcumin targeting spinal cord injury, Biomed. Pharmacother. 159 (2023) 114224.

[32] C. Tang, Q. Wang, K. Li, X. Li, C. Wang, L. Xue, C. Ju, C. Zhang, A neutrophil-mimetic magnetic nanoprobe for molecular magnetic resonance imaging of stroke-induced neuroinflammation, Biomater. Sci. 9 (15) (2021) 5247–5258.

[33] L. Li, B. Han, Y. Wang, J. Zhao, Y. Cao, Simple and universal signal labeling of cell surface for amplified detection of cancer cells via mild reduction, Biosens. Bioelectron. 145 (2019) 111714.

[34] D. Wang, H. Dong, M. Li, Y. Cao, F. Yang, K. Zhang, W. Dai, C. Wang, X. Zhang, Erythrocyte-Cancer hybrid membrane camouflaged hollow copper sulfide nanoparticles for prolonged circulation life and homotypic-targeting photothermal/chemotherapy of melanoma, ACS Nano 12 (6) (2018) 5241–5252.

[35] X. Wu, Y.P. Zhang, W. Qu, L.B.E. Shields, C.B. Shields, X.M. Xu, A tissue displacement-based contusive spinal cord injury model in mice, J. Vis. Exp. 124 (2017).

[36] M.J. Farrar, I.M. Bernstein, D.H. Schlafer, T.A. Cleland, J.R. Fetcho, C.B. Schaffer, Chronic in vivo imaging in the mouse spinal cord using an implanted chamber, Nat. Methods 9 (3) (2012) 297–302.

[37] K. Chen, H. Nishi, R. Travers, N. Tsuboi, K. Martinod, D.D. Wagner, R. Stan, K. Croce, T.N. Mayadas, Endocytosis of soluble immune complexes leads to their clearance by FcgammaRIIIB but induces neutrophil extracellular traps via FcgammaRIIA in vivo, Blood 120 (22) (2012) 4421–4431.

[38] X. Wu, W. Qu, A.A. Bakare, Y.P. Zhang, C.M.E. Fry, L.B.E. Shields, C.B. Shields, X. M. Xu, A laser-guided spinal cord displacement injury in adult mice, J. Neurotrauma 36 (3) (2019) 460–468.

[39] V. Brinkmann, U. Reichard, C. Goosmann, B. Fauler, Y. Uhlemann, D.S. Weiss, Y. Weinrauch, A. Zychlinsky, Neutrophil extracellular traps kill bacteria, Science 303 (5663) (2004) 1532–1535.

[40] N. Wei, T. Lu, L. Yang, Y. Dong, X. Liu, Lipoxin A4 protects primary spinal cord neurons from Erastin-induced ferroptosis by activating the Akt/Nrf2/HO-1 signaling pathway, FEBS Open Bio 11 (8) (2021) 2118–2126.

[41] H. Kim, K. Shin, O.K. Park, D. Choi, H.D. Kim, S. Baik, S.H. Lee, S.H. Kwon, K. J. Yarema, J. Hong, T. Hyeon, N.S. Hwang, General and facile coating of single cells via mild reduction, J. Am. Chem. Soc. 140 (4) (2018) 1199–1202.

[42] W. Xie, P. Liu, F. Gao, Y. Gu, Y. Xiao, P. Wu, B. Chen, W. Liu, Q. Liu, Platelet-neutrophil hybrid membrane-coated gelatin nanoparticles for enhanced targeting ability and intelligent release in the treatment of non-alcoholic steatohepatitis, Nanomedicine. 42 (2022) 102538.

[43] V. Sreeramkumar, J.M. Adrover, I. Ballesteros, M.I. Cuartero, J. Rossaint, I. Bilbao, M. Nacher, C. Pitaval, I. Radovanovic, Y. Fukui, R.P. McEver, M.D. Filippi, I. Lizasoain, J. Ruiz-Cabello, A. Zarbock, M.A. Moro, A. Hidalgo, Neutrophils scan for activated platelets to initiate inflammation, Science 346 (6214) (2014) 1234–1238.

[44] S. Dolma, H. Kumar, Neutrophil, extracellular matrix components, and their interlinked action in promoting secondary pathogenesis after spinal cord injury, Mol. Neurobiol. 58 (9) (2021) 4652–4665.

[45] T. Liu, L. Zhang, D. Joo, S.C. Sun, NF-kappaB signaling in inflammation, Signal Transduct. Targeted Ther. 2 (2017) 17023.

[46] R.H. Shih, C.Y. Wang, C.M. Yang, NF-kappaB signaling pathways in neurological inflammation: a mini review, Front. Mol. Neurosci. 8 (2015) 77.

[47] H. Ni, W. Jin, T. Zhu, J. Wang, B. Yuan, J. Jiang, W. Liang, Z. Ma, Curcumin modulates TLR4/NF-kappaB inflammatory signaling pathway following traumatic spinal cord injury in rats, J Spinal Cord Med. 38 (2) (2015) 199–206.

[48] E.R. Akhmetzyanova, M.N. Zhuravleva, A.V. Timofeeva, L.G. Tazetdinova, E. E. Garanina, A.A. Rizvanov, Y.O. Mukhamedshina, Severity- and time-dependent activation of microglia in spinal cord injury, Int. J. Mol. Sci. 24 (9) (2023).

[49] S.A. Quadri, M. Farooqui, A. Ikram, A. Zafar, M.A. Khan, S.S. Suriya, C.F. Claus, B. Fiani, M. Rahman, A. Ramachandran, I.I.T. Armstrong, M.A. Taqi, M. M. Mortazavi, Recent update on basic mechanisms of spinal cord injury, Neurosurg. Rev. 43 (2) (2020) 425–441.

[50] L. Lossi, C. Castagna, A. Merighi, Caspase-3 mediated cell death in the normal development of the mammalian cerebellum, Int. J. Mol. Sci. 19 (12) (2018).

[51] C. Zhang, D. Guo, H. Qiao, J. Li, J. Li, Y. Yang, S. Chang, F. Li, D. Wang, H. Li, X. He, F. Wang, Macrophage extracellular traps exacerbate secondary spinal cord injury by modulating macrophage/microglia polarization via LL37/P2X7R/NF-kappaB signaling pathway, Oxid. Med. Cell. Longev. 2022 (2022) 9197940.

[52] J.Y. Wei, M.Y. Hu, X.Q. Chen, J.S. Wei, J. Chen, X.K. Qin, F.Y. Lei, J.S. Zou, S. Q. Zhu, Y.H. Qin, Hypobaric hypoxia aggravates renal injury by inducing the formation of neutrophil extracellular traps through the NF-kappaB signaling pathway, Curr Med Sci 43 (3) (2023) 469–477.

[53] J. Chen, T. Wang, X. Li, L. Gao, K. Wang, M. Cheng, Z. Zeng, L. Chen, Y. Shen, F. Wen, DNA of neutrophil extracellular traps promote NF-kappaB-dependent autoimmunity via cGAS/TLR9 in chronic obstructive pulmonary disease, Signal Transduct. Targeted Ther. 9 (1) (2024) 163.

[54] Y.Y. Lee, H.H. Park, W. Park, H. Kim, J.G. Jang, K.S. Hong, J.Y. Lee, H.S. Seo, D. H. Na, T.H. Kim, Y.B. Choy, J.H. Ahn, W. Lee, C.G. Park, Long-acting nanoparticulate DNase-1 for effective suppression of SARS-CoV-2-mediated neutrophil activities and cytokine storm, Biomaterials 267 (2021) 120389.

[55] L. Alekseeva, N. Mironova, Role of cell-free DNA and deoxyribonucleases in tumor progression, Int. J. Mol. Sci. 22 (22) (2021).

[56] L.C. Penaloza Arias, D.N. Huynh, S. Babity, S. Marleau, D. Brambilla, Optimization of a liposomal DNase I formulation with an extended circulating half-life, Mol. Pharm. 19 (6) (2022) 1906–1916.

[57] Y. Du, Y. Chen, F. Li, Z. Mao, Y. Ding, W. Wang, Genetically engineered cellular nanovesicle as targeted DNase I delivery system for the clearance of neutrophil extracellular traps in acute lung injury, Adv. Sci. 10 (32) (2023) e2303053.